Identification of a 35S U4/U6.U5 tri-small nuclear ribonucleoprotein (tri-snRNP) complex intermediate in spliceosome assembly

Received for publication, May 17, 2017, and in revised form, August 28, 2017 Published, Papers in Press, September 6, 2017, DOI 10.1074/jbc.M117.797357

Zhe Chen[‡], Bin Gui[‡], Yu Zhang[‡], Guojia Xie[‡], Wanjin Li[‡], Shumeng Liu[‡], Bosen Xu[‡], Chongyang Wu[‡], Lin He[‡], Jianguo Yang[‡], Xia Yi[‡], Xiaohan Yang[‡], Luyang Sun[‡], Jing Liang[‡], and Yongfeng Shang[‡§¶1]

From the [‡]Key Laboratory of Carcinogenesis and Translational Research (Ministry of Education), Department of Biochemistry and Molecular Biology, School of Basic Medical Sciences, Peking University Health Science Center, Beijing 100191, China, the [§]Department of Biochemistry and Molecular Biology, School of Basic Medical Sciences, Tianjin Medical University, Tianjin 300070, China, and the [¶]Department of Biochemistry and Molecular Biology, School of Basic Medical Sciences, Capital Medical University, Beijing 100069, China

Edited by Ronald C. Wek

The *de novo* assembly and post-splicing reassembly of the U4/U6.U5 tri-snRNP remain to be investigated. We report here that ZIP, a protein containing a CCCH-type zinc finger and a G-patch domain, as characterized by us previously, regulates pre-mRNA splicing independent of RNA binding. We found that ZIP physically associates with the U4/U6.U5 tri-small nuclear ribonucleoprotein (tri-snRNP). Remarkably, the ZIP-containing tri-snRNP, which has a sedimentation coefficient of ~35S, is a tri-snRNP that has not been described previously. We also found that the 35S tri-snRNP contains hPrp24, indicative of a state in which the U4/U6 di-snRNP is integrating with the U5 snRNP. We found that the 35S tri-snRNP is enriched in the Cajal body, indicating that it is an assembly intermediate during 25S tri-snRNP maturation. We showed that the 35S tri-snRNP also contains hPrp43, in which ATPase/RNA helicase activities are stimulated by ZIP. Our study identified, for the first time, a tri-snRNP intermediate, shedding new light on the *de novo* assembly and recycling of the U4/U6.U5 tri-snRNP.

The removal of introns from pre-messenger RNA (pre-mRNA) is a prerequisite for the expression of most eukaryotic genes. Nuclear pre-mRNA splicing is catalyzed by a large dynamic ribonucleoprotein complex, the spliceosome (1, 2). This molecular machinery is assembled *de novo* on each intron to be spliced. To facilitate this process, a major portion of the engaged proteins is preassembled into a number of small nuclear ribonucleoprotein (snRNP)[2] modules, each centered on one or more small nuclear RNA (snRNA) molecules (3–5).

This work was supported by Grants 91219201, 81530073, and 81730079 from the National Natural Science Foundation of China (to Y. S.) and Grant 2016YFC1302304 from the Ministry of Science and Technology of China (to Y. S.). The authors declare that they have no conflicts of interest with the contents of this article.

This article contains supplemental File 1 and Tables S1 and S2.

[1] To whom correspondence should be addressed: Dept. of Biochemistry and Molecular Biology, Peking University Health Science Center, 38 Xueyuan Rd., Beijing 100191, China. Tel.: 86-10-82801608; Fax: 86-10-82801355; E-mail: yshang@hsc.pku.edu.cn.

[2] The abbreviations used are: snRNP, small nuclear ribonucleoprotein; ESE, exon-splicing enhancer; bis-Tris, 2-[bis(2-hydroxyethyl)amino]-2-(hydroxymethyl)propane-1,3-diol; TRITC, tetramethylrhodamine isothiocyanate; CV, column volume.

The spliceosome assembly is an ordered and stepwise process that involves dynamic snRNP–snRNP and snRNP–pre-mRNA interactions in which snRNPs U1 and U2 interact first through RNA base-pairing with the intron at the 5′-splice site and branch point sequence, respectively (6–10). This is followed by binding of the U4/U6.U5 tri-snRNP (11–13). The spliceosome then undergoes a major remodeling, releasing U1 and U4 and forming new base pairs between U6 and the 5′-splice site and between U2 and U6 (14–16). Subsequently, a Prp19-contaning protein complex joins the spliceosome to stabilize the specific interaction of U5 and U6 with pre-mRNA, generating an activated spliceosome (17–19).

After the excision of each intron, the spliceosome is completely dismantled, a process leaving many of the participating complexes altered either in structure or composition (1, 2, 20). Specifically, the U4/U6.U5 tri-snRNP is thought to disband into individual snRNPs U4, U5, and U6 following the splicing reactions (20–22). Reentry into a new cycle therefore requires that these snRNPs reunite as a tri-snRNP. It is believed that the recycling of the U4/U6 di-snRNP requires a conserved auxiliary factor, Prp24 in yeast and hPrp24 or p110 in humans, which associates with U6 snRNP to facilitate the annealing of U4 and U6 snRNAs (23, 24). Interestingly, Prp24 dissociates from U4/U6 di-snRNP prior to or concomitantly with the association of U4/U6 di-snRNP with U5 snRNP and thus is not a part of the U4/U6.U5 tri-snRNP (24). The ternary complex between U4 and U6 snRNAs and Prp24 is relatively stable (25), implying that mechanism/factor(s) is required for the displacement of Prp24 *in vivo*.

The assembly of the U4/U6 di-snRNP and the U4/U6.U5 tri-snRNP is thought to take place in the Cajal body (26–29). It is relatively clear how U4/U6 di-snRNP is assembled, at least *in vitro*, where hPrp24 and LSm proteins promote the annealing of U4 and U6 snRNA (24, 30) and hSnu13 binds to the 5′ stem loop of the U4 snRNA to nucleate U4/U6 di-snRNP–specific proteins (31). However, the molecular events involved in the integration of U4/U6 di-snRNP with U5 snRNP and the formation of mature tri-snRNP are still not fully understood, especially *in vivo*. The tri-snRNP purified from HeLa cells contains, in addition to U4, U6, and U5 snRNAs, ~30 distinct protein

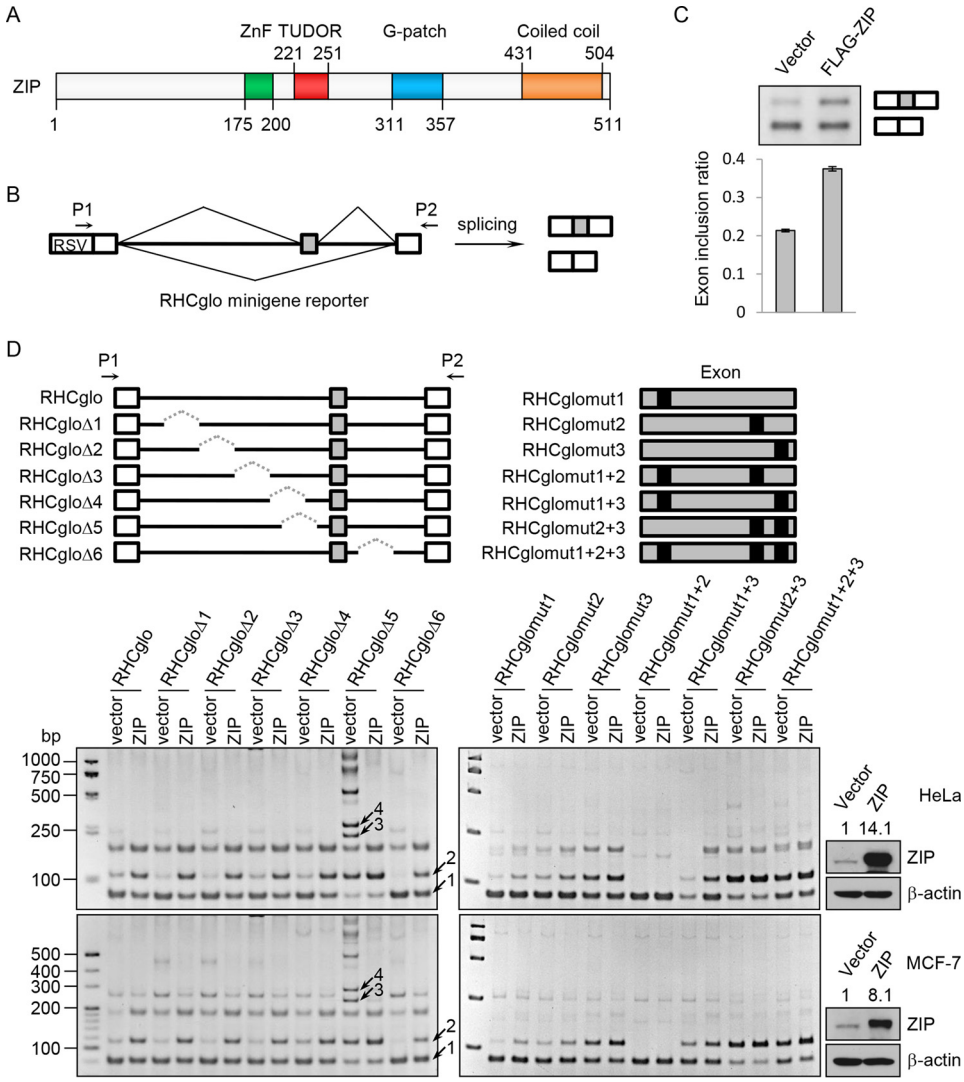

Figure 1. ZIP regulates pre-mRNA splicing independent of RNA binding. *A*, schematic representation of the structure of ZIP. *ZnF*, CCCH-type zinc finger. *B*, schematic illustration of the RHCglo minigene reporter. The alternatively spliced middle exon is indicated by a *gray box*. *C*, HeLa cells were co-transfected with the RHCglo minigene and ZIP or empty vector, splicing of the RHCglo minigene was determined by semiquantitative RT-PCR, and the results were quantified by densitometry. *D*, HeLa and MCF-7 cells were co-transfected with the RHCglo minigene or its mutants as well as ZIP or empty vector, and splicing of the RHCglo minigene or its mutants was determined by semiquantitative RT-PCR. Bands marked by *arrows* are true splicing products confirmed by TA cloning and sequencing, and other bands are aberrant PCR products. ZIP overexpression was analyzed by Western blotting and quantified by densitometry.

species (32, 33). It is thought that protein–protein interactions, especially the interaction between hPrp31 and hPrp6, play a role in the association of U4/U6 di-snRNP with U5 snRNP (28, 33), and an early study shows that when incubated with proteins stripped from stable 25S tri-snRNP, isolated 20S U5 snRNP assemble with 10S U4/U6 snRNP to form a stable 25S tri-snRNP *in vitro* (32). Nevertheless, the molecular events leading to the release of hPrp24 from U4/U6 di-snRNP and the incorporation of tri-snRNP–specific proteins into tri-snRNP remain unclear.

Previously, we cloned and characterized a gene, *ZIP* (for zinc finger and G-patch domain–containing protein), from a mammary cDNA library (34). ZIP harbors a CCCH-type zinc finger and a G-patch domain, both of which are characteristic of proteins implicated in mRNA processing and turnover (35–43), suggesting a role for ZIP in RNA metabolism. In this study, we identified a 35S tri-snRNP, which contains ZIP, hPrp24, and hPrp43. We showed that the 35S tri-snRNP is enriched in the Cajal body. We demonstrated that ZIP stimulates the ATPase and RNA helicase activities of hPrp43 and propose that this action is functionally linked to the releasing of hPrp24 during the assembly of the U4/U6.U5 tri-snRNP.

Results

ZIP regulates pre-mRNA splicing independent of RNA binding

As stated above, ZIP contains a CCCH-type zinc finger and a G-patch domain (Fig. 1*A*), structural modules often seen in proteins involved in mRNA processing and turnover, which suggests a role for ZIP in RNA metabolism. To investigate whether ZIP is functionally involved in mRNA processing, we first used the RHCglo minigene as a reporter (44) to examine the effect of ZIP on pre-mRNA splicing. The RHCglo minigene has three exons (Fig. 1*B*), and the middle exon is skipped in most transcripts. Upon ZIP overexpression, we detected, by semiquantitative RT-PCR, a significant increase in the inclu-

sion of the middle exon in HeLa cells co-transfected with the RHCglo minigene reporter (Fig. 1*C*), suggesting that ZIP is involved in the regulation of alternative splicing.

As splicing regulators typically bind to a specific RNA sequence and recruit spliceosome machinery to the nearby splice sites in their regulation of splicing (45–47), and as ZIP contains a CCCH-type zinc finger capable of binding DNA/RNA, to gain further support of the notion that ZIP regulates pre-mRNA splicing, we constructed a series of deletion mutants of the RHCglo minigene reporter to map the sequence responsible for ZIP's splicing-enhancing function (Fig. 1*D*). The deletion mutants of the RHCglo minigene reporter were co-transfected with ZIP in HeLa cells, and the effect of ZIP on the splicing of these constructs was measured by RT-PCR. The results showed that ZIP had a similar impact on the splicing of the RHCglo minigene reporter constructs, except for RHCgloΔ5, which had the middle exon inclusion even in the absence of ZIP (Fig. 1*D*), which might have resulted from the interruption of the intron-splicing silencer of the middle exon (45–47). These results suggest that ZIP regulates RHCglo minigene splicing independent of binding to the intron. Notably, in addition to the major spliced transcripts, we found two other splicing products (bands 3 and 4), especially for the RHCgloΔ5 minigene reporter, and remarkably, the overexpression of ZIP resulted in the inhibition of these two splicing products (Fig. 1*D* and supplemental File 1). As ZIP might also bind to the exon of RHCglo minigene, we constructed a series of Exon-splicing enhancer (ESE) mutants to examine whether ZIP functions by binding to the exon of RHCglo minigene (Fig. 1*D*). To this end, ESE mutants of the RHCglo minigene reporter were co-transfected with ZIP in HeLa cells, and the effect of ZIP on the splicing of these constructs was measured by RT-PCR. The results showed that ZIP affected the splicing of the RHCglo minigene reporter constructs in a similar fashion, except for RHCglomut1 + 2, which skipped the middle exon even when ZIP was overexpressed (Fig. 1*D*). However, this was probably due to the destruction of the middle exon by the ESE mutation itself, as no leaky splicing of the middle exon was detected in the RHCglomut1 + 2 minigene. These results suggest that ZIP regulates RHCglo minigene splicing independent of binding to the exon. Similar results were obtained when the experiments were carried out in MCF-7 cells (Fig. 1*D*). These results indicate that ZIP enhances the middle exon inclusion independent of RNA binding and helps exon definition, implying that ZIP regulates pre-mRNA splicing by acting as an atypical splicing regulator through alternative mechanisms.

ZIP is physically associated with tri-snRNP

To gain mechanistic insights into the regulation of splicing by ZIP, we utilized epitope-based proteomic screening with combined immunopurification and mass spectrometry to interrogate the ZIP interactome *in vivo*. To this end, we established a HeLa cell line stably expressing FLAG-tagged ZIP (FLAG-ZIP). Immunoaffinity purification was performed on whole-cell lysis with anti-FLAG–agarose, and the ZIP-containing complex was eluted under native conditions with excess FLAG peptides. The eluates were resolved on SDS-PAGE, and protein bands were silver-stained and retrieved. Mass spectrometry consistently identified a series of proteins including all U4/U6.U5 tri-snRNP proteins known currently, as well as several other proteins including hPrp24 and hPrp43 (Fig. 2*A* and supplemental Table S1), suggesting that ZIP is physically associated with the U4/U6.U5 tri-snRNP *in vivo*. In support of this notion, detection by Northern blotting of RNAs that were extracted from anti-FLAG immunoprecipitates revealed that indeed U4, U5, and U6 snRNAs, but not U1 and U2, were co-purified with ZIP (Fig. 2*B*).

To further support the deduction that ZIP is physically associated with the U4/U6.U5 tri-snRNP *in vivo*, total proteins from HeLa cells were extracted, and co-immunoprecipitation experiments were performed with antibodies detecting endogenous proteins. Immunoprecipitation with antibodies against ZIP followed by immunoblotting with antibodies against hPrp8, hBrr2, hSnu114, hPrp3, or hSad1 (U4/U6.U5 tri-snRNP proteins) or against U1–70K (U1 snRNP protein) or SF3a66 (U2 snRNP protein) revealed that the protein components of the U4/U6.U5 tri-snRNP, but not of the U1 and U2 snRNPs, could be co-immunoprecipitated efficiently with ZIP (Fig. 2*C*). Reciprocally, immunoprecipitation with antibodies against representative proteins of the tri-snRNP, U1 snRNP, or U2 snRNP followed by immunoblotting with antibodies against ZIP also revealed that ZIP was effectively co-immunoprecipitated with the protein components of the U4/U6.U5 tri-snRNP but not with that of U1 and U2 snRNPs (Fig. 2*C*). Together, these results indicate that ZIP is physically associated with the U4/U6.U5 tri-snRNP *in vivo*.

Identification of a 35S tri-snRNP containing ZIP, hPrp24, and hPrp43

In addition to U4/U6.U5 tri-snRNP proteins, hPrp24 and hPrp43 were also identified in the ZIP-containing complex in immunopurification and mass spectrometry experiments with a high coverage (supplemental Table S1). hPrp24 is a chaperone protein in the assembly of the U4/U6 di-snRNP (23, 24). It is found in U6 snRNP and U4/U6 di-snRNP but not in U4/U6.U5 tri-snRNP (24). hPrp43 is an ATPase and DEAH RNA helicase implicated in the disassembly of the spliceosome as well as the biogenesis of the ribosome (48–52). The enzymatic activity of its yeast orthologue, Prp43, is regulated by G-patch domain–containing proteins (38, 39, 42). In addition, hPrp43 also has been identified in 17S U2 snRNP in HeLa cells (53). To confirm the *in vivo* interaction of ZIP with hPrp24 and hPrp43, total proteins from HeLa cells were extracted, and co-immunoprecipitation experiments were performed. Immunoprecipitation with antibodies against ZIP followed by immunoblotting with antibodies against hPrp24 or hPrp43 showed that hPrp24 and hPrp43 could be efficiently co-immunoprecipitated with ZIP (Fig. 3*A*). Reciprocally, immunoprecipitation with antibodies against hPrp24 or hPrp43 followed by immunoblotting with antibodies against ZIP also revealed that ZIP co-immunoprecipitated with hPrp24 and hPrp43 (Fig. 3*A*).

To further substantiate the observation that ZIP is physically associated with the U4/U6.U5 tri-snRNP as well as with hPrp24 and hPrp43, and to reconcile the observation that ZIP interacts with hPrp24 but hPrp24 is only found in U6 and U4/U6 snRNPs and not in the U4/U6.U5 tri-snRNP (24), immunoaffinity puri-

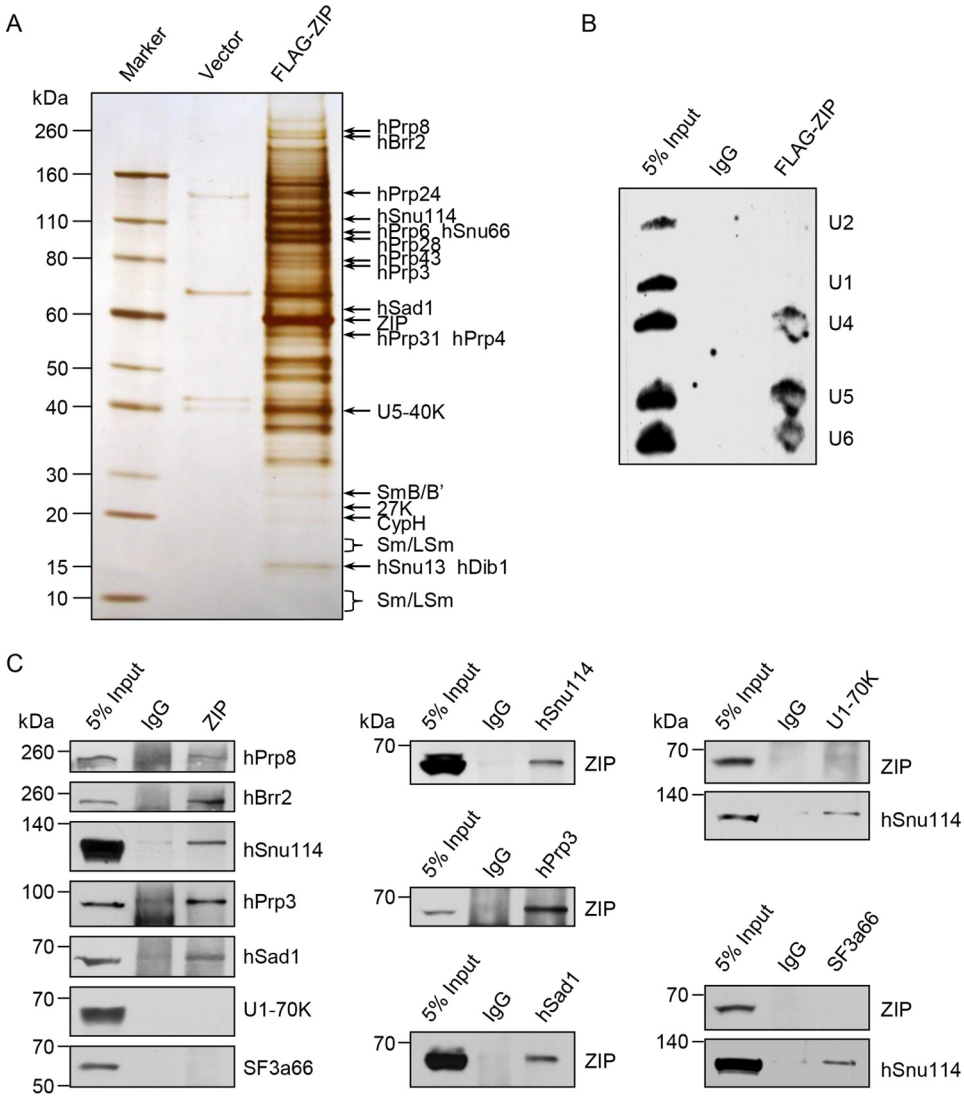

Figure 2. ZIP is physically associated with tri-snRNP. *A*, mass spectrometry analysis of ZIP-associated proteins. Whole-cell extracts from HeLa cells stably expressing FLAG-ZIP were prepared and subjected to affinity purification with anti-FLAG antibody that was immobilized on agarose beads. The purified protein complexes were resolved on SDS-PAGE and silver-stained, and the bands were retrieved and analyzed by mass spectrometry. Detailed results from the mass spectrometry analysis are provided in supplemental Table S1. *B*, Northern blotting analysis of ZIP-associated snRNAs. RNAs were extracted with phenol/chloroform from the anti-FLAG–purified ZIP-associated complex, precipitated with ethanol, and resolved on a 6% denaturing gel. The blot was then transferred onto nylon membrane and hybridized with U1, U2, U4, U5, and U6 probes. *C*, co-immunoprecipitation analysis of ZIP-associated snRNP proteins. Whole-cell lysates from HeLa cells were prepared, and immunoprecipitation was performed with anti-ZIP followed by immunoblotting with antibodies against the indicated representative proteins of snRNPs (*left*) or with antibodies against hSnu114, hPrp3, hSad1, U1–70K, or SF3a66 followed by immunoblotting with anti-ZIP (*right*).

fication was performed again in HeLa cells stably expressing FLAG-ZIP. The bound complexes were eluted under native conditions with excess FLAG peptides and fractionated on 10–30% glycerol gradients at 32,000 rpm for 16 h, as described elsewhere (24), to separate hPrp24-containing U4/U6 di-snRNP and U4/U6.U5 tri-snRNP. Proteins were isolated from gradient fractions and analyzed by SDS-PAGE and silver staining (Fig. 3*B*). To our surprise, we found that the ZIP-containing complex resided primarily on the bottom fraction with a sedimentation coefficient larger than 23S. Examination of the distribution of hPrp24, hPrp43, and representative protein components of tri-snRNP including hSnu114, hPrp3, and hSad1 across the gradient by Western blotting of total proteins recovered from gradient fractions showed that hPrp24, hPrp43, and the tri-snRNP proteins were also mainly detected at the bottom fraction with a sedimentation coefficient larger than 23S (Fig. 3*C*). Notably, hPrp24 and hPrp3 had a second peak with a sedimentation coefficient of about 14S (Fig. 3*C*, fractions 12–14), close to U4/U6 di-snRNP sedimentation coefficient of ~13S (54), which is consistent with the notion that hPrp24 is associated with U4/U6 snRNP (24).

Given the observation that the ZIP-containing complex was larger than 23S, we thus tried to fractionate the immunopurification eluates on 10–30% glycerol gradients at a lower speed, 25,000 rpm, for 16 h. Analysis of the proteins retrieved from gradient fractions by SDS-PAGE and silver staining showed that the ZIP-containing complex had a sedimentation coefficient around 35S (Fig. 3*D*, *fractions 15–17*). Analysis of the distribution of hPrp24, hPrp43, and the representative protein components of tri-snRNP across the gradient by Western blot-

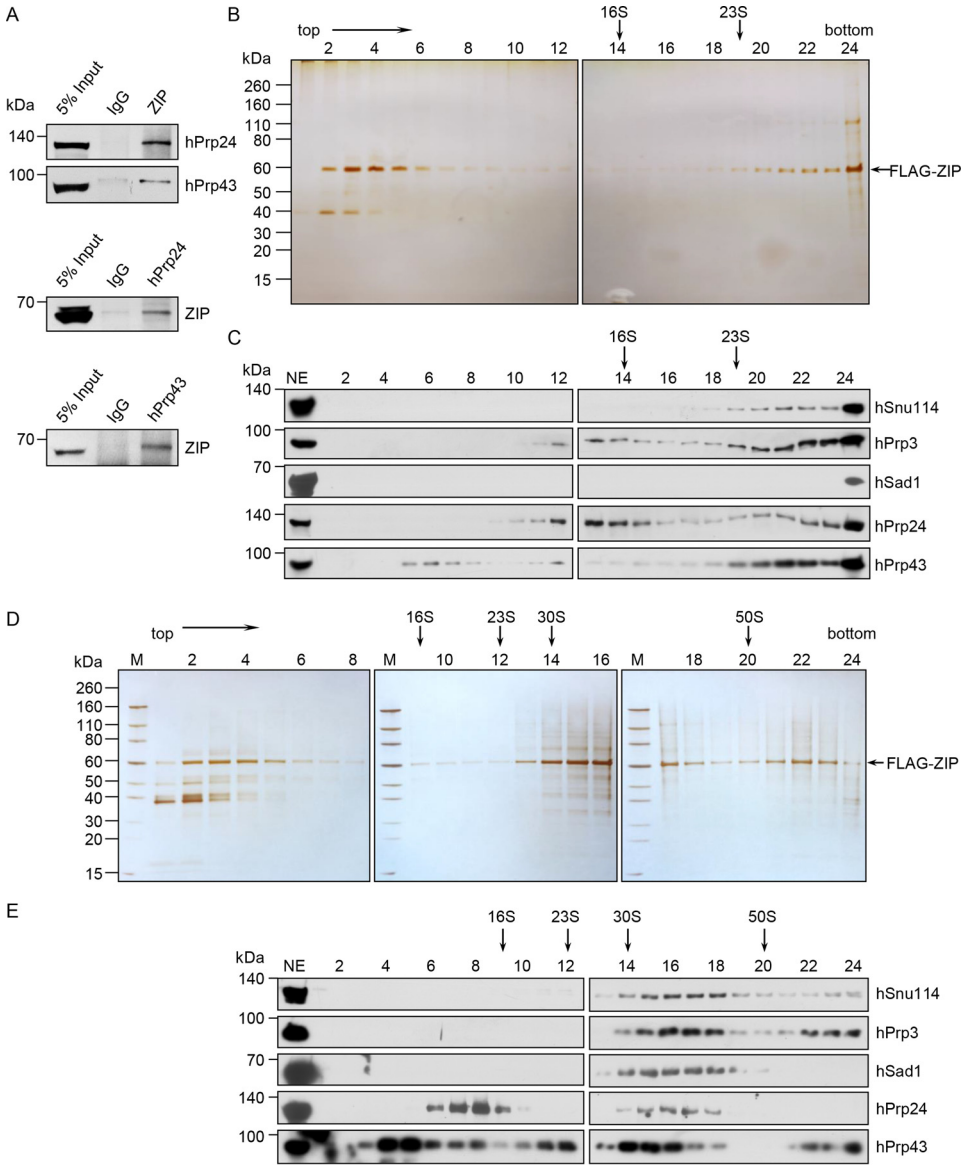

Figure 3. identification of a 35S tri-snRNP containing ZIP, hPrp24, and hPrp43. *A*, ZIP associates with hPrp24 and hPrp43 *in vivo*. Whole-cell lysates from HeLa cells were prepared, and immunoprecipitation was performed with anti-ZIP followed by immunoblotting with antibodies against hPrp24 or hPrp43 or with antibodies against hPrp24 or hPrp43 followed by immunoblotting with anti-ZIP. *B*, ZIP-containing complex is larger than 23S. Affinity-purified ZIP-associated complexes were fractionated on 10–30% glycerol gradients at 32,000 rpm for 16 h. Proteins from each fraction were resolved on SDS-PAGE and silver-stained. *C*, ZIP, hPrp24, and tri-snRNP proteins coexist in a complex larger than 23S. Affinity-purified ZIP-associated complexes were fractionated on 10–30% glycerol gradients at 32,000 rpm for 16 h. Proteins from each fraction were resolved on SDS-PAGE and subjected to Western blot analysis. *D*, ZIP-containing complex has a sedimentation coefficient of ~35S. Affinity-purified ZIP-associated complexes were fractionated on 10–30% glycerol gradients at 25,000 rpm for 16 h. Proteins from each fraction were resolved on SDS-PAGE and silver-stained, and the bands of fractions 15–16, corresponding to 35S, were retrieved and analyzed by mass spectrometry. Detailed results from the mass spectrometry analysis are provided in supplemental Table S2. *E*, ZIP, hPrp24, hPrp43, and tri-snRNP proteins coexist in the ~35S complex. Affinity-purified ZIP-associated complexes were fractionated on 10–30% glycerol gradients at 25,000 rpm for 16 h. Proteins from each fraction were resolved on SDS-PAGE and subjected to Western blot analysis.

ting demonstrated that, consistent with the results of silver staining, the major peak of hSnu114, hPrp3, and hSad1, respectively, was detected in fractions 15–17, corresponding to the main peak of ZIP, whereas hPrp24 had two peaks, one at fractions 15–17 corresponding to the peak of ZIP and the tri-snRNP proteins and the other at fractions 7–8 with a sedimentation coefficient of about 14S (Fig. 3*E*), consistent with the results described above. Importantly, although hPrp43 displayed a more extended distribution, it had a peak that overlapped with that of ZIP and the tri-snRNP proteins (Fig. 3*E*). Significantly, mass spectrometric analysis of the proteins in fractions 15–16 confirmed the existence of ZIP, hPrp24, hPrp43, hSnu114, hPrp3, and hSad1 as well as nearly all other currently known tri-snRNP proteins (supplemental Table S2). Collectively, these results support the conclusion that ZIP, hPrp24, and hPrp43, three proteins not reported in the U4/U6.U5 tri-snRNP previously, are associated with the U4/U6.U5 tri-snRNP *in vivo*.

The existence of stable 35S tri-snRNP particles in vivo

To further support the existence of the 35S tri-snRNP particle *in vivo*, we next assessed the strength of the interaction

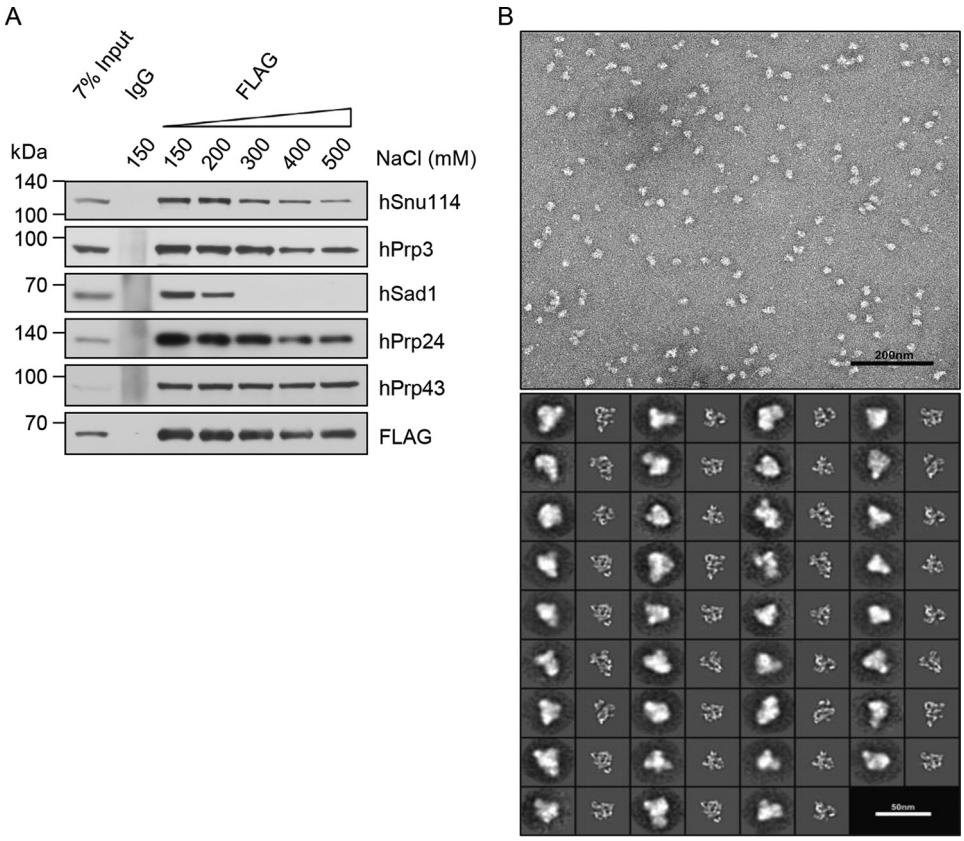

Figure 4. The existence of stable 35S tri-snRNP particles *in vivo*. *A*, the 35S tri-snRNP is stable at the physiological concentration of NaCl. Affinity-purified ZIP-associated 35S tri-snRNP was washed with salt solutions with different stringencies, resolved on SDS-PAGE, and subjected to Western blot analysis. *B*, electron micrograph of negatively stained 35S ZIP-containing complex. The 35S ZIP-containing complex was separated and fixed using the GraFix procedure, negatively stained with uranyl formate, and analyzed by electron microscopy (*upper panel*). Shown is a comparison of typical views of the 35S ZIP-containing complex aligned and classified using IMAGIC-4D software with reprojections of human 25S tri-snRNP (EMD-1257) (*lower panel*).

between the components of the 35S U4/U6.U5 tri-snRNP. To this end, the immunoaffinity-purified ZIP-containing complex was washed using solutions of different ionic strengths. Western blot analysis showed that the 35S tri-snRNP was stable at the physiological concentration of NaCl (Fig. 4*A*). Tri-snRNP-specific hSad1 started to dissociate at 200 mM NaCl, consistent with a previous report (55), and hSnu114 was retained in the complex until NaCl concentration rose to >300 mM, in accordance with a previous report that tri-snRNP disassembles into U5 and U4/U6 particles at a high-salt concentration (56). Evidently, although hPrp3 and hPrp24 started to leave the complex when the NaCl concentration was higher than 400 mM, hPrp43 was more stable and associated with ZIP even when the NaCl concentration reached 500 mM. These observations suggest that the 35S tri-snRNP is as stable as the canonical 25S tri-snRNP. Collectively, these findings support the existence of a 35S U4/U6.U5 tri-snRNP *in vivo*, which appears to represent a state in which U4/U6 di-snRNP is just integrating with U5 snRNP and when hPrp24 is yet to leave during tri-snRNP maturation. This concept is supported by the presence of the ATPase/RNA helicase hPrp43 in the 35S tri-snRNP, which implies that the 35S tri-snRNP is subjected to further remodeling.

To further support the existence of 35S tri-snRNP particle *in vivo*, affinity-purified ZIP-containing complexes were subjected to GraFix (57), negatively stained with uranyl formate, and analyzed by electron microscopy. These experiments revealed that the 35S ZIP-containing complex displayed a monodispersed particle distribution under negative staining electron microscopy (Fig. 4*B*). Analysis by reference-free single-particle 2D alignment and classification using IMAGIC-4D software demonstrated that although 35S tri-snRNP particles could not be determined specifically, ZIP-containing particles displayed typical views that resemble 3D model reprojections of the humans 25S U4/U6.U5 tri-snRNP (Fig. 4*B*).

The 35S tri-snRNP is enriched in the Cajal body

The tri-snRNP that has been recognized thus far is the 25S form of tri-snRNP (32); the 35S tri-snRNP containing ZIP, hPrp24, and hPrp43 has not been reported previously. The 25S tri-snRNP is assembled and matured in the Cajal body (28, 29). The act of splicing breaks the tri-snRNP into individual snRNPs, which are then recycled back to the Cajal body for reassembly before another round of splicing (58). It is reported that whereas hPrp24-containing U6 snRNP is localized exclusively in the nucleoplasm, hPrp24-containing U4/U6 di-snRNP preferentially resides in the Cajal body (26, 27). To further confirm the existence of the 35S tri-snRNP and to define its biological significance, we next determined the subcellular localization of the 35S tri-snRNP by tracking its associated proteins in cells. Analysis by immunofluorescent confocal microscopy of HeLa cells double-labeled with anti-ZIP and anti-coilin showed

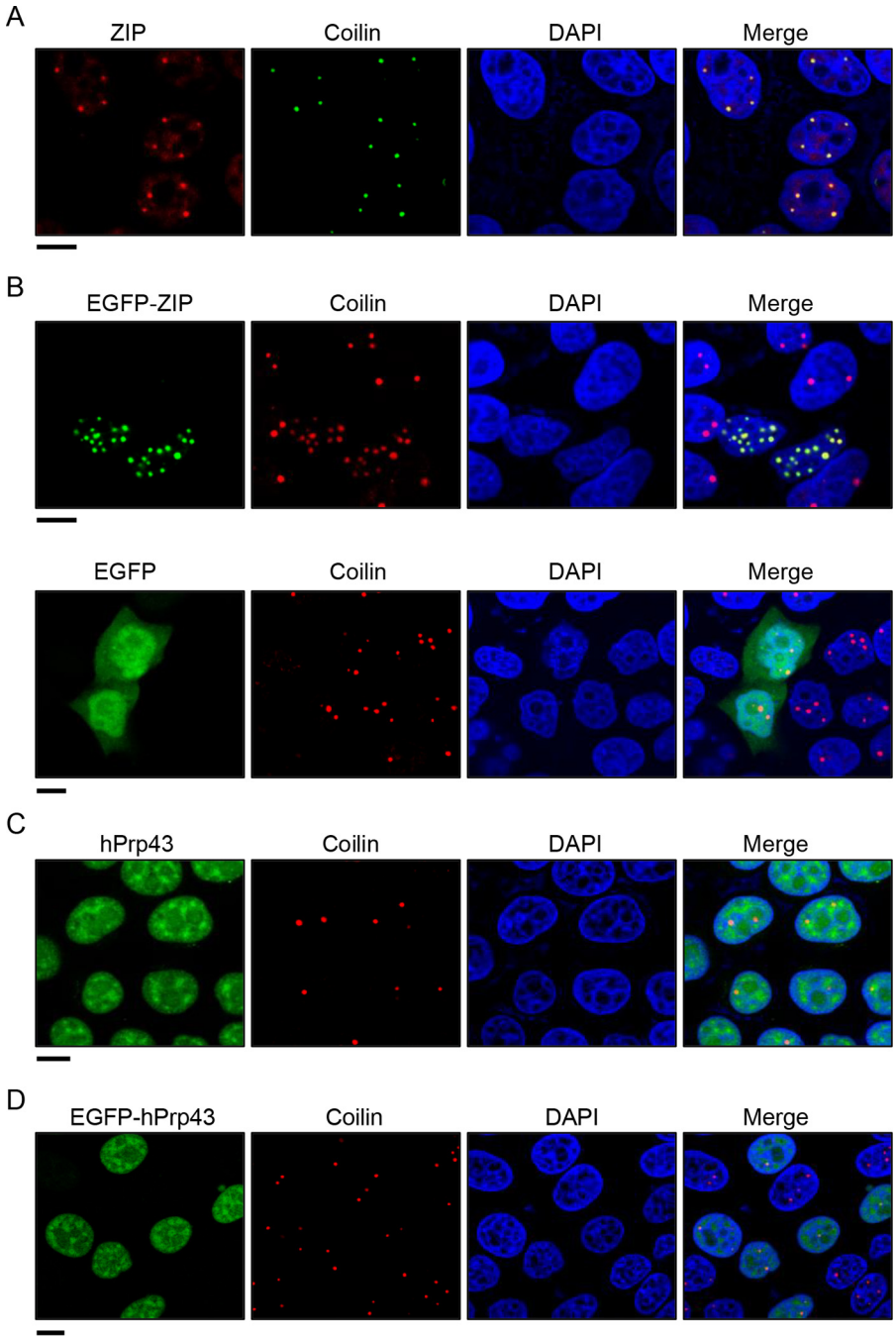

Figure 5. The 35S tri-snRNP is enriched in the Cajal body. *A*, HeLa cells were immunostained with antibodies against ZIP and coilin and analyzed by confocal microscopy. *B*, HeLa cells were transfected with EGFP-ZIP or EGFP and immunostained with antibodies against coilin and analyzed by confocal microscopy. *C*, HeLa cells were immunostained with antibodies against hPrp43 and coilin and analyzed by confocal microscopy. *D*, HeLa cells were transfected with EGFP-hPrp43 and immunostained with antibodies against coilin and analyzed by immunofluorescent microscopy. *Scale bars*: 10 μm.

that ZIP was detected exclusively in the nucleus where it was distributed throughout the nucleoplasm yet enriched in large bright dots (Fig. 5*A*). Remarkably, these dots completely overlapped with the staining of coilin, an unambiguous marker for the Cajal body (59) (Fig. 5*A*). Similar results were obtained in HeLa cells expressing EGFP-tagged ZIP (Fig. 5*B*). Meanwhile, analysis by immunofluorescent confocal microscopy of HeLa cells double-labeled with anti-hPrp43 and anti-coilin revealed that hPrp43 was also distributed throughout the nucleoplasm, enriched in nuclear speckles, and overlapped with coilin (Fig. 5*C*), in agreement with a previous report that hPrp43 accumulates in nuclear speckles in HEp-2 cells (60). Similar results were obtained in HeLa cells expressing EGFP-tagged hPrp43 (Fig. 5*D*). Together, these results indicate that the 35S tri-snRNP is enriched in the Cajal body, suggesting that the 35S tri-snRNP is an intermediate during 25S tri-snRNP maturation.

Notably, overexpression of ZIP (EGFP-tagged ZIP) resulted in an increase, compared with overexpression of EGFP only, in the number of Cajal bodies in the nucleus (Fig. 5*B*). As it has been reported that the rate of U4/U6 di-snRNP assembly is ~11-fold faster (61) and tri-snRNP assembly is ~10-fold faster in the Cajal body than in the surrounding nucleoplasm (62), it is

possible that the ZIP overexpression-associated increase in the number of Cajal bodies is functionally linked to the regulation of the splicing of the RHCglo minigene by ZIP.

ZIP interacts with hPrp3 and hPrp43 in the 35S tri-snRNP

To further support the existence of a tri-snRNP intermediate and to investigate the functional role of ZIP in tri-snRNP maturation, we next investigated the molecular interaction of ZIP in tri-snRNP. To this end, the genes encoding for the 35S tri-snRNP proteins hPrp3, hPrp4, hPrp31, and hPrp43 were cloned first from a HeLa cDNA library. Bacterially expressed GST-ZIP was purified and incubated with *in vitro* transcribed/translated hPrp3, hPrp4, hPrp31, or hPrp43. We found that ZIP interacted with hPrp3 and hPrp43 but not hPrp4 or hPrp31 (Fig. 6*A*). Further analysis by GST pulldown assays with bacterially expressed GST-tagged ZIP deletion mutants and *in vitro* transcribed/translated hPrp3 or hPrp43 demonstrated that the G-patch domain of ZIP was responsible for its interaction with hPrp43 and the N-terminal 140 amino acids of ZIP were necessary for its interaction with hPrp3 (Fig. 6*C*).

Structurally, hPrp3 contains three domains: the middle domain binds to the U4/U6 double helix, the C-terminal domain binds to single-stranded U6 RNA (63–66), and the function of the N-terminal domain of hPrp3 is not known. In addition, hPrp24 has also been reported to interact with the middle domain of hPrp3 (67). However, the function of the N-terminal domain of hPrp3 has not been defined (Fig. 6*D*). Immunoprecipitation in HeLa cells transfected with FLAG-tagged deletion mutants of hPrp3 with anti-FLAG followed by immunoblotting with anti-ZIP showed that although the N-terminal domain-deleted hPrp3 mutant could interact with hPrp24, it no longer interacted with ZIP (Fig. 6*D*), indicating that the N-terminal domain of hPrp3 is responsible for interaction with ZIP. This means that hPrp3 could interact with both ZIP and hPrp24.

To understand the functional significance of the physical interaction between ZIP and hPrp3, we investigated the influence of the hPrp3 interaction sequence of ZIP on the subcellular localization of ZIP in the Cajal body. Analysis by immunofluorescent confocal microscopy of HeLa cells transfected with EGFP-tagged ZIP or ZIP deletion mutants showed that the N-terminal domain– deleted ZIP, ZIPΔ1–140, which lacks the sequence responsible for ZIP interaction with hPrp3, failed to be localized in the Cajal body; it displayed a dispersed distribution pattern in the nucleus, whereas the G-patch-deleted ZIP mutant, ZIPΔG-patch, retained its ability to be localized in the Cajal body (Fig. 6*E*). These results indicate that the physical interaction of ZIP with hPrp3 is required for the localization of ZIP in the Cajal body, suggesting that ZIP is recruited to the 35S tri-snRNP by hPrp3.

To understand the functional significance of the physical interaction between ZIP and hPrp43, we first performed co-immunoprecipitation experiments in HeLa cells transfected with FLAG-tagged ZIP deletion mutants. Immunoprecipitation with anti-FLAG followed by immunoblotting with antibodies against 35S tri-snRNP proteins revealed that none of the tested 35S tri-snRNP proteins could be immunoprecipitated with ZIPΔ1–140, whereas all of the tested 35S tri-snRNP proteins, including hPrp43, could be efficiently immunoprecipitated with ZIPΔG-patch (Fig. 6*F*), suggesting that the recruitment of hPrp43 to the tri-snRNP intermediate does not depend on ZIP, reminiscent of the relationship between Spp2 and Prp2 in the B^{act} spliceosome (40).

We then performed the RHCglo minigene reporter assays again. Co-transfection of ZIP or its deletion mutants and the RHCglo minigene in HeLa cells and analysis by RT-PCR indicated that both ZIPΔ1–140 and ZIPΔG-patch lost their ability to enhance the inclusion of the middle exon in the RHCglo minigene (Fig. 6*G*); this implies that physical interaction of ZIP with both hPrp3 and hPrp43 is required for the splicing regulatory function of ZIP. We found that ZIPΔTUDOR also lost its ability to enhance the inclusion of the middle exon in the RHCglo minigene (Fig. 6*G*). As the TUDOR domain is located between the 1–140–amino acid sequence and the G-patch domain, the ZIPΔTUDOR mutant would alter the relative spatial positioning of the 1–140 sequence and the G-patch domain, leading to a loss of interaction of the ZIPΔTUDOR mutant with hPrp3 or/and hPrp43 and thus a loss of function of ZIP.

ZIP stimulates the ATPase and RNA helicase activities of hPrp43

hPrp43 possesses both ATPase and RNA helicase activities (68), thought to be important for the remodeling of the tri-snRNP intermediate. To further explore the functional significance of the physical interaction between ZIP and hPrp43, we next tested whether ZIP could influence the enzymatic activities of hPrp43. To this end, the rate of ATP hydrolysis by hPrp43 was measured as a function of ATP concentration in the absence of RNA and in the presence of ZIP or ZIPΔG-patch. Consistent with its yeast homologue (49), hPrp43 exhibited little ATPase activity when incubated with ATP only. The maximal rate of ATP hydrolysis by hPrp43 at 0.5 mM ATP in this condition was only 0.15 ± 0.09/min (mol ATP/mol protein/min) (Fig. 7*A*). However, when ZIP was added to the reaction, the maximal rate of ATP hydrolysis at 0.5 mM ATP increased to 10.3 ± 2.0/min, whereas the addition of ZIPΔG-patch did not result in any appreciable changes in the rate of ATP hydrolysis by hPrp43 (Fig. 7*A*). ZIP itself had no detectable ATPase activity. These results indicate that interacting with ZIP increases the ability of hPrp43 to hydrolyze ATP in the absence of RNA.

As the ATPase activity of its yeast homologue, Prp43, was dependent on the RNA cofactor (49), we thus added saturating concentrations of synthetic RNA_{40} to hPrp43 reaction. The rate of ATP hydrolysis at 0.5 mM ATP by hPrp43 was elevated to 13.7 ± 1.5/min by the inclusion of RNA_{40}. The addition of ZIP further increased the rate of ATP hydrolysis at 0.5 mM ATP to 86.2 ± 1.1/min, whereas the addition of ZIPΔG-patch had negligible effects on the rate of ATP hydrolysis by hPrp43 (Fig. 7*B*). Synthetic RNA_{40} itself had no detectable ATPase activity in the absence of hPrp43. These results indicate that ZIP and RNA synergistically stimulate the ATPase activity of hPrp43.

To examine the effect of ZIP on the RNA helicase activity of hPrp43, we constructed two RNA-DNA hybrids, containing a 3′- or 5′-single–stranded tail, respectively, to allow detection of 3′–5′ or 5′–3′ unwinding. Helicase assays were performed by mixing the 3′-tailed or 5′-tailed substrates with hPrp43 and ATP in the presence or absence of ZIP or ZIPΔG-patch. The

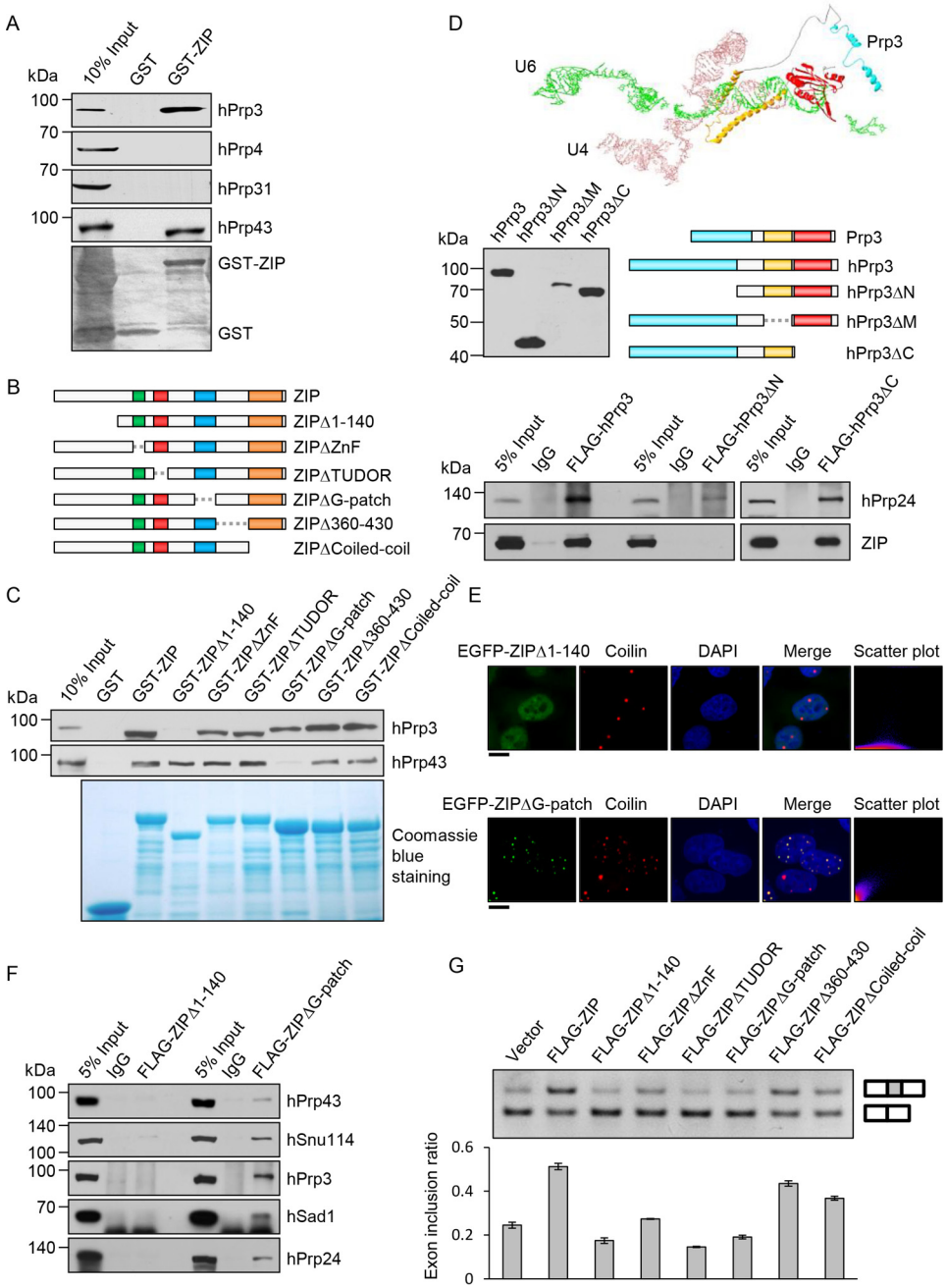

Figure 6. ZIP interacts with hPrp3 and hPrp43 in the 35S tri-snRNP. *A*, ZIP interacts with hPrp3 and hPrp43 *in vitro*. GST pulldown assays were performed with GST-ZIP and *in vitro* transcribed/translated components of the 35S tri-snRNP. *B*, schematic representation of ZIP deletion mutants used in GST pulldown, immunofluorescent staining, immunoprecipitation, and splicing reporter assays. *C*, the N-terminal and G-patch domains of ZIP interact with hPrp3 and hPrp43, respectively. GST pulldown assays were performed with GST-tagged ZIP or its mutants and *in vitro* transcribed/translated hPrp3 or hPrp43. *D*, the N-terminal domain of hPrp3 is essential for its interaction with ZIP. HeLa cells were transfected with FLAG-tagged hPrp3 or its mutants. Cellular lysates were prepared and immunoprecipitated with anti-FLAG followed by immunoblotting with antibodies against ZIP or hPrp24. The structure of Prp3 was analyzed using the yeast tri-snRNP structure 5GAN. Deletion mutants of hPrp3 were constructed according to the structure of the Prp3 in tri-snRNP, and their expression in HeLa cells was examined. *E*, HeLa cells were transfected with EGFP-ZIPΔ1–140 or EGFP-ZIPΔG-patch, stained with antibodies against coilin, and analyzed by confocal microscopy. *Scale bars*: 10 μm. The Pearson correlation coefficient of colocalization of EGFP-ZIPΔ1–140 and EGFP-ZIPΔG-patch with coilin was 0.32 $\pm$ 0.02 and 0.76 $\pm$ 0.01, respectively, based on ImageJ. *F*, HeLa cells were transfected with FLAG-tagged ZIPΔ1–140 or ZIPΔG-patch. Cellular lysates were prepared and immunoprecipitated with anti-FLAG followed by immunoblotting with antibodies against the indicated components of the 35S tri-snRNP. *G*, both the N-terminal and G-patch domains of ZIP are required for inclusion of the middle exon of the RHCglo minigene. HeLa cells were co-transfected with the RHCglo minigene and ZIP or its mutants. Splicing of the RHCglo minigene was determined by semiquantitative RT-PCR, and the results were quantified by densitometry.

unwinding of the substrates was analyzed by native polyacrylamide gel electrophoresis. In the absence of ZIP, no hPrp43-mediated unwinding was detected for the 3′-tailed substrate, and although a certain degree of unwinding was detected for the 5′-tailed substrate, it might have resulted from the instability of the 5′-tailed substrate itself, as it partly unwound even in the absence of ATP (Fig. 7*C*). However, when ZIP was included in the reaction, both the 3′-tailed and 5′-tailed substrates were

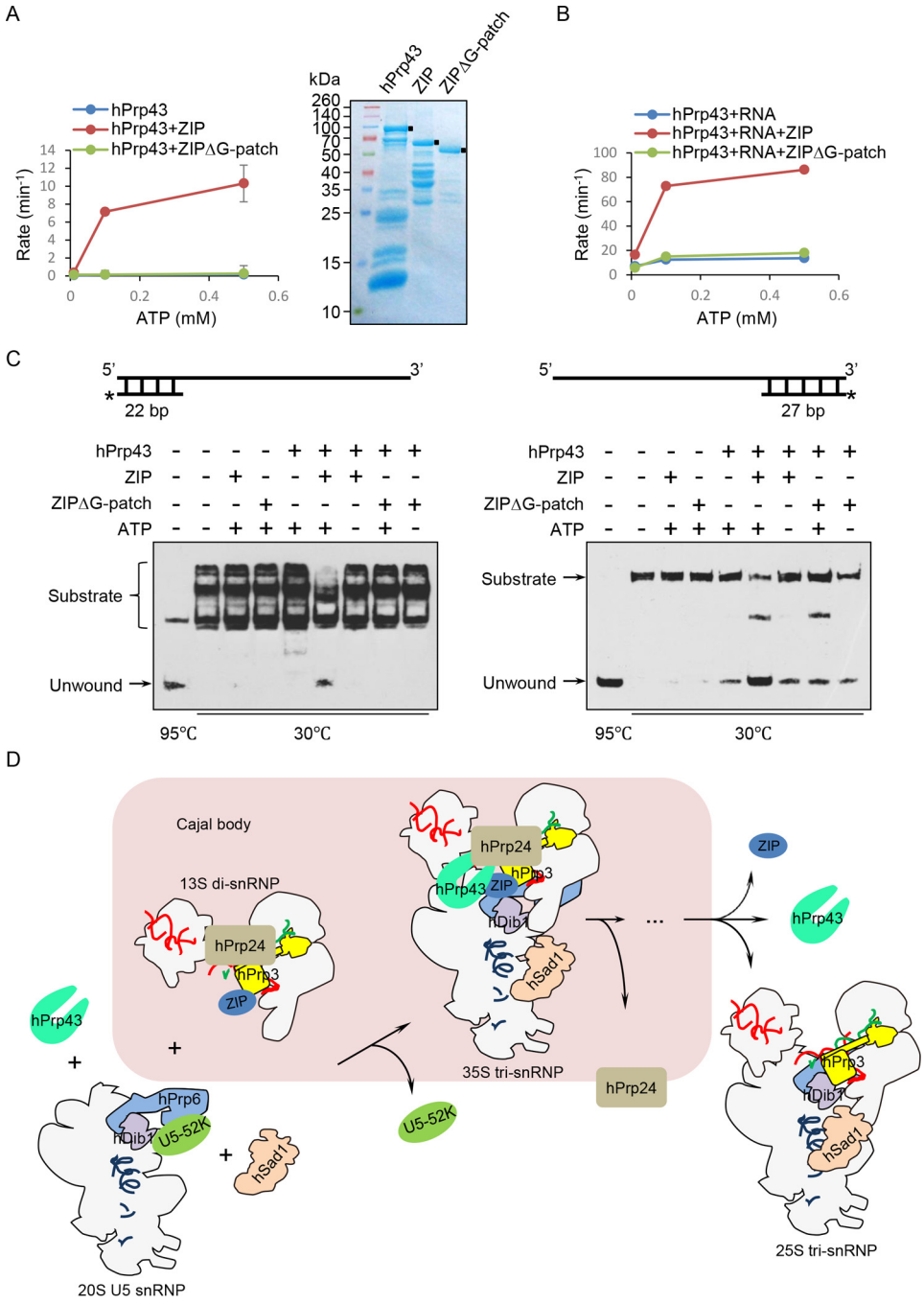

Figure 7. ZIP stimulates ATPase and RNA helicase activities of hPrp43. *A*, ZIP stimulates ATP hydrolysis by hPrp43. ATPase assays were performed with 0.01, 0.1, or 0.5 mM ATP and 100 nM hPrp43 in the absence or presence of 100 nM ZIP or ZIPΔG-patch. Purified recombinant proteins were analyzed by SDS-PAGE and Coomassie Blue staining. *B*, ATPase assays for hPrp43 in the presence of a 40-nt synthetic RNA (500 nM). Data are presented as means ± S.D. for three independent measurements. *C*, ZIP stimulates the helicase activity of hPrp43. RNA helicase assays were performed with 3′-tailed (*left*) or 5′-tailed substrates (*right*) under the indicated conditions. *D*, the proposed model for the U5 snRNP integrating with the U4/U6 di-snRNP. ZIP is recruited to the U4/U6 di-snRNP by hPrp3 first in the Cajal body. The ZIP-containing U4/U6 di-snRNP is then integrated with the 20S U5 snRNP, tri-snRNP-specific proteins, and hPrp43 to form the 35S tri-snRNP. After remodeling, hPrp24 is released and ZIP and hPrp43 dissociate to generate a more mature tri-snRNP.

efficiently unwound (Fig. 7*C*). No hPrp43-mediated unwinding of either substrate was detected when ZIPΔG-patch was included in the reaction (Fig. 7*C*). These results indicate that ZIP stimulates the RNA helicase activity of hPrp43 and that the G-patch domain of ZIP is required for this stimulation.

Discussion

Although the assembly of the U4/U6.U5 tri-snRNP, especially the assembly of the U4/U6 di-snRNP, has been studied intensively *in vitro* (1, 2, 4, 5) and the final stage of U4/U6.U5 tri-snRNP maturation was found to take place in the Cajal body more than 10 years ago (28), the molecular events involved in the maturation of the tri-snRNP *in vivo* remain to be delineated. Previously, we cloned and characterized the *ZIP* gene, and we reported at the time that ZIP interacts with the chromatin-remodeling NuRD complex and functions in transcription regulation (34). Based on the structural characterization that ZIP contains a CCCH-type zinc finger and a G-patch domain, both

of which are signatory motifs of proteins implicated in RNA processing and turnover (35–43), in the current study we investigated the possible role of ZIP in RNA metabolism. We found that ZIP promotes the inclusion of the middle exon of the RHC-glo minigene reporter, suggesting that ZIP is a splicing regulator. Consistent with this notion, a high-throughput screening for factors that enhance FGFR2 splicing found that ZIP is the most potent facilitator of the inclusion of the middle exon of the PKC-neg-40B-IF3-Luc minigene reporter (69). Moreover, we found that ZIP regulates splicing independent of RNA binding, suggesting that ZIP is an atypical splicing regulator and may be an snRNP-associated protein. Indeed, mechanistic studies revealed that ZIP is physically associated with the U4/U6.U5 tri-snRNP. Remarkably, we found that the ZIP-associated tri-snRNP has a sedimentation coefficient of about 35S.

The U4/U6.U5 tri-snRNP that has been recognized thus far is the 25S form (32); the 35S tri-snRNP has not been reported previously. We found that the 35S tri-snRNP contains ZIP, hPrp24, and hPrp43, three proteins that have not been reported in tri-snRNP previously. As it is believed that hPrp24 exists only in U6 and U4/U6 di-snRNP, but not in U4/U6.U5 tri-snRNP (24), and a recent report found that hPrp24 functions to monitor tri-snRNP assembly by sequestering incomplete particles in the Cajal body (29), the detection of hPrp24 in ZIP-associated tri-snRNP suggests that the 35S tri-snRNP may represent a state in which U4/U6 di-snRNP is just integrating with U5 snRNP. If this interpretation is correct, it means that the 35S U4/U6.U5 tri-snRNP is an intermediate of the 25S U4/U6.U5 tri-snRNP. Two lines of evidence support this proposition. First, the existence of hPrp43, a DEAH RNA helicase, in the 35S tri-snRNP implies that this assembly is a complex subjecting to further remodeling; and second, the 35S tri-snRNP is enriched in the Cajal body, where the final steps of tri-snRNP maturation take place (28, 29). Compared with the canonical 25S tri-snRNP, the additional 10S sedimentation coefficient of the 35S tri-snRNP may result from an extended conformation of a non-compact state. Thus, the larger sedimentation coefficient itself might reflect that the 35S tri-snRNP is an incomplete assembly of the mature 25S tri-snRNP.

The snRNP and spliceosomal proteins have been investigated extensively over the last 28 years with the help of mass spectrometry (70). So, it is hard to imagine that there are still missing proteins in snRNPs and the spliceosome. However, as RNAs and protein components of snRNPs are constantly associated with/dissociated from snRNPs or spliceosome, and as snRNPs and the spliceosome undergo dynamic assembly/disassembly, it is nevertheless possible that the 35S tri-snRNP has evaded detection up to now.

Prp43, the yeast homologue of hPrp43, was initially described as a disassembly factor of the spliceosome required for the release of a spliced-out lariat intron from the U2/U5/U6 post-spliceosome and for the disassembly of this post-spliceosome (21, 48, 49). It is also proposed that Prp43 acts to maintain the fidelity of the splicing reaction by rejecting suboptimal substrates during spliceosome assembly (71, 72). In addition, it is reported that Prp43 is associated with pre-ribosomal particles from the initial transcriptional steps of the pre-rRNA to the last maturation steps of the pre-ribosomal particles in the cytoplasm (50–52), suggesting that Prp43 is also involved in ribosome biogenesis. Moreover, hPrp43 has also been identified in the 17S U2 snRNP in humans, although its function in this complex is unclear (53). We report in the current study that hPrp43 is a component of the 35S tri-snRNP, supporting the functional versatility of this protein in RNA metabolism. hPrp43 is a DEAH RNA helicase. In past years, mounting evidence has indicated that G-patch–containing proteins interact with DEAH RNA helicases Prp43 and Prp2 in yeast and humans and modulate the NTPase and RNA helicase activities of Prp43 and Prp2 *in vitro* (37–40, 42, 43, 68, 73). Consistently, we have demonstrated in the current study that ZIP, a G-patch–containing protein, stimulates the ATPase and RNA helicase activities of hPrp43. We found that, intriguingly, although ZIP is capable of interacting with hPrp43, the recruitment of hPrp43 to the 35S tri-snRNP appears to be independent of ZIP. This kind of relationship has also been reported for Spp2 and Prp2 in the B^{act} spliceosome (40). Moreover, as mentioned above, hPrp43 also exists in the 17S U2 snRNP, which includes two G-patch–containing proteins, CHERP and SPF45 (53). It is conceivable that CHERP and SPF45 function to influence the activities of hPrp43 during U2 snRNP assembly or the branch point recognition during spliceosome assembly. Clearly, more studies are needed to understand the relationship between the structure and function of G-patch domain–containing proteins, especially in the context of RNA metabolism. In addition, target analysis for Prp43 in yeast by CRAC UV cross-linking has determined that it is involved mainly in pre-rRNA processing and targets U6 snRNA (74). Given the complexity of the human spliceosome and ribosome, it will be interesting to identify the targets of hPrp43 in human cells.

hPrp24 protein is required for the annealing of U4 and U6 snRNAs (23, 24). It forms a stable ternary complex with U4 and U6 thereafter (25) but is not found in mature tri-snRNP (24). Another U4/U6 di-snRNP protein, hPrp3, contains three domains, with the middle domain binding to the U4/U6 double helix and the C-terminal domain binding to single-stranded U6 RNA (63, 64, 66). In addition, the middle domain of hPrp3 also interacts with hPrp24 (67). However, the function of the N-terminal domain of hPrp3 is unknown. In this study, we found that the N-terminal domain of hPrp3 interacts with the N terminus of ZIP. Because ZIP also interacts with hPrp43 through its G-patch domain, the molecular interactions among hPrp3, hPrp24, ZIP, and hPrp43 point to a scenario that brings hPrp24 and hPrp43 to a short distance within the 35S tri-snRNP. As hPrp24 is not found in mature 25S tri-snRNP (24) and thus must leave before 25S tri-snRNP maturation, it is plausible to postulate that hPrp43 is functionally linked to the departure of hPrp24 in 35S tri-snRNP. Based on this idea and on our finding that there exists a ~14S ZIP- and hPrp24-containing di-snRNP when ZIP-containing complexes are separated, we propose that ZIP is recruited to the U4/U6 di-snRNP by hPrp3 first. It is then integrated with the 20S U5 snRNP, tri-snRNP-specific proteins, and hPrp43 to form a 35S tri-snRNP in the Cajal body, where hPrp24 dissociates after remodeling and ZIP and hPrp43 also depart to generate a more mature tri-snRNP (Fig. 7*D*).

We also tested the effect of loss-of-function ZIP on the splicing of the minigene reporter and found that ZIP depletion

had no significant influence on the splicing of the minigene reporter. There is no ZIP homologue in yeast, and whether functionally redundant proteins exist in humans is currently unknown. After all, not all cell types harbor the Cajal body (75). Thus, it is possible that the biogenesis and recycling of the tri-snRNP occurs through alternative pathways in cells that have no Cajal bodies. We did not detect any overt phenotype in the *ZIP* knock-out mouse either. This is rather surprising but is reminiscent of *Coilin* knock-out. Coilin is the backbone and marker of the Cajal body (59). *Coilin* disruptions in plants and flies have no detectable effect on viability or fertility (76, 77), and *Coilin* null mice have no appreciable abnormalities (78, 79). Therefore, the possibility that ZIP regulates splicing in a tissue-specific manner or environmentally dependent fashion cannot be excluded. Hopefully, future investigations will be able to address these issues. Moreover, the functional relationship between transcription regulation (34) and tri-snRNP assembly of ZIP is currently unclear, and whether these processes involve alternatively spliced ZIP awaits further elucidations. Nevertheless, we report in the current study the identification of a previously undescribed 35S U4/U6.U5 tri-snRNP. We found that this tri-snRNP contains ZIP, hPrp24, and hPrp43. We demonstrated that ZIP acts to stimulate the enzymatic activity of hPrp43 and thus propose that this stimulation may be functionally linked to the releasing of hPrp24.

Materials and methods

Antibodies and plasmids

The antibodies used were: anti-hPrp8 (11171-1-AP), anti-hBrr2 (23875-1-AP), anti-hSnu114 (10208-1-AP), anti-hSad1 (23865-1-AP), anti-SF3a66 (15596-1-AP), and anti-hPrp24 (18025-1-AP) from Proteintech; anti-hPrp3 (sc-102068), anti-U1–70K (sc-390899), and anti-coilin (sc-55594) from Santa Cruz Biotechnology; anti-hPrp43 (A300–390A) from Bethyl; and anti-FLAG (F3165) from Sigma. Polyclonal antibodies against ZIP were raised against purified recombinant ZIP (1–200 amino acids) in rabbits by GenScript. The RHCglo minigene reporter was kindly provided by Thomas A. Cooper (Baylor College of Medicine) (44). Deletion mutants of the RHCglo minigene reporter were constructed by overlapping PCR. ESEs of the middle exon were predicted by ESEfinder (80), and the middle four bases of each ESE motif were mutated to ACCA. Wild-type and deletion mutants of ZIP were amplified by PCR and inserted into pcDNA3.1(−) with an N-terminal FLAG tag or into the pET-42a(+) or pEGFP-N1 vector. The cDNA for hPrp3, hPrp4, hPrp31, and hPrp43 was amplified by PCR and inserted into the pcDNA3.1(−) vector with an N-terminal FLAG tag. Deletion mutants of hPrp3 were generated by subcloning the corresponding fragments of hPrp3 into the pcDNA3.1(−) vector with an N-terminal FLAG tag. To purify proteins for hPrp43 enzymatic activity assays, the cDNA for hPrp43, ZIP, and ZIPΔG-patch was subcloned into a modified pSUMO-pET-28a(+) vector. All clones were confirmed by DNA sequencing.

Cell culture and transfection

HeLa and MCF-7 cell lines were obtained from ATCC. Cells were maintained in DMEM (Hyclone) supplemented with 10% FBS. Transfections were carried out using Lipofectamine 2000 (Invitrogen) according to the manufacturer's instruction.

RT-PCR

Total RNAs were isolated from cells with TRIzol reagent (Invitrogen). Any potential DNA contamination was removed by treatment with RNase-free DNase (Promega). First-strand cDNA was synthesized with the reverse transcription system (Promega, A3500). PCR was performed with TNIE4 (5′-AGGTGCTGCCGCCGGGCGGTGGCTG-3′) and RSV5U (5′-CATTCACCACATTGGTGTGC-3′) primers, resolved on a 5% polyacrylamide gel, and stained with SYBR Gold (Invitrogen). The identity of the splicing variants was confirmed by TA cloning and DNA sequencing.

Immunopurification, silver staining, and mass spectrometry

The HeLa cell line stably expressing FLAG-tagged ZIP was generated by infecting HeLa cells with lentiviruses carrying FLAG-tagged ZIP and selected with 1.5 μg/ml puromycin. Cellular lysates were obtained from $\sim 5 \times 10^8$ cells lysed in cold Nonidet P-40 buffer (50 mM Tris-HCl, pH 7.6, 150 mM NaCl, 0.5% Nonidet P-40) plus protease inhibitors (Roche Applied Science) for 30 min at 4 °C. This was followed by centrifugation at 14,000 $\times$ *g* for 20 min at 4 °C. The protein supernatant was incubated with anti-FLAG M2 gel (Sigma) for 2 h at 4 °C. After washing with cold Nonidet P-40 buffer five times, FLAG-peptides (Sigma) were used to elute the protein complex from the gel following the manufacturer's instruction. The eluted protein complexes were then resolved on NuPAGE, 4–12% bis-Tris gel (Invitrogen), stained with a Pierce silver-staining kit, and subjected to LC-MS/MS (LTQ Orbitrap Elite) sequencing and data analysis.

Northern blotting

Total RNAs were extracted with phenol/chloroform from the affinity-purified protein complexes, precipitated with ethanol, and subjected to electrophoresis on a 6% urea denaturing gel. The blot was then transferred onto a nylon membrane (Hybond-N+, GE Healthcare), hybridized with U1, U2, U4, U5, and U6 biotin-labeled DNA probes, and detected by using a chemiluminescent nucleic acid detection module kit (Thermo Scientific Pierce). The probe sequences were: U1, 5′-TCCCCTGCCAGGTAAGTATC-3′; U2, 5′-TTAGCCAAAAGGCCGAGAAGCGAT-3′; U4, 5′-GGGGTATTGGGAAAAGTTTTC-3′; U5, 5′-GATTTATGCGATCTGAAGAGAAACC-3′; and U6, 5′-TTCTCTGTATCGTTCCAAT-3′.

Immunoprecipitation and Western blotting

For immunoprecipitation experiments, HeLa cells were lysed in cold Nonidet P-40 buffer plus protease inhibitors for 30 min at 4 °C followed by centrifugation at 13,200 $\times$ *g* for 15 min at 4 °C. The protein supernatant was incubated with 1 μg of specific antibodies for 12 h at 4 °C with constant rotation; 50 μl of 50% protein A– or G–agarose beads (GE Healthcare) was then added, and the incubation was continued for an additional 2 h. The beads were then washed five times with the Nonidet P-40 buffer. Between washes, the beads were collected by centrifugation at 500 $\times$ *g* for 5 min at 4 °C. The precipitated pro-

teins were eluted from the beads by resuspending the beads in 2× SDS-PAGE loading buffer and boiling them for 10 min. The resultant materials from immunoprecipitation or cellular lysates were then resolved using 8% SDS-PAGE and transferred onto nitrocellulose membranes. For Western blotting, membranes were incubated with the appropriate antibodies overnight at 4 °C followed by incubation with an HRP-conjugated secondary antibody (Jackson ImmunoResearch). Immunoreactive bands were visualized using Western blotting Luminol reagent (Santa Cruz Biotechnology) according to the manufacturer's recommendation.

Glycerol gradient sedimentation

For fractionation of ZIP-containing complexes, 400 μl of eluted complexes was loaded onto an 11-ml glycerol gradient (10–30% (v/v) glycerol in buffer G (20 mM HEPES-KOH, pH 7.9, 150 mM NaCl, 1.5 mM $MgCl_2$)). After ultracentrifugation (32,000 or 25,000 rpm, Beckman SW 40 Ti rotor) at 4 °C for 16 h, 500 μl of fractionated materials were retrieved from top to bottom of the gradient. Sedimentation markers used were 16S and 23S rRNA (Roche Applied Science) and 30S and 50S ribosome subunits (New England Biolabs). Proteins from each fraction were resolved on SDS-PAGE and subjected to silver staining or Western blot analysis.

Negative-staining EM and image processing

The 35S ZIP-containing complex was separated and fixed using the GraFix procedure (57) on a 4-ml linear 10–30% (v/v) glycerol and 0%-0.1% (v/v) glutaraldehyde gradient in buffer G. Samples were negatively stained in 2% (w/v) uranyl acetate (Electron Microscopy Sciences) solution following the standard deep-stain procedure on holey carbon-coated EM copper grids covered with a thin layer of continuous carbon. Then, negatively stained specimens were examined by a Tecnai Spirit electron microscope operated at 120-kV acceleration voltage, and magnified digital micrographs of the specimens were taken on a Gatan UltraScan 4000 CCD camera. Reference-free 2D alignment and classification were performed using IMAGIC-4D (81), and the results were compared with reprojections of humans 25S tri-snRNP structure (EMD-1257) (82).

Immunofluorescent microscopy

HeLa cells grown on 6-well chamber slides were fixed in 4% paraformaldehyde, washed with PBS, permeabilized with 0.2% Triton X-100, blocked with 0.8% BSA, and incubated with the appropriate primary antibodies followed by staining with FITC- or TRITC-conjugated secondary antibodies (Jackson ImmunoResearch). Cells were then washed four times, and a final concentration of 0.1 μg/ml DAPI (Sigma) was included in the final wash to stain the nuclei. Images were visualized and recorded with an Olympus FV1000S confocal microscope. For detection of EGFP constructs in the cells, fixation was done 36 h after transfection.

GST pulldown assay

GST fusion constructs were expressed in *Escherichia coli* bacteria. Crude bacterial lysates were prepared by sonication in TEDGN (50 mM Tris-HCl, pH 7.4, 1.5 mM EDTA, 1 mM dithiothreitol, 10% (v/v) glycerol, 0.4 M NaCl) in the presence of the protease inhibitor mixture. *In vitro* transcription/translation was carried out with rabbit reticulocyte lysate (TNT Systems, Promega) according to the manufacturer's recommendation. In GST pulldown assays, about 4 μg of the appropriate GST fusion proteins was mixed with 8 μl of the *in vitro* transcribed/translated products and incubated in binding buffer (150 mM NaCl, 50 mM HEPES, pH 7.9) at room temperature for 30 min in the presence of the protease inhibitor mixture. The binding reaction was then added to 30 μl of glutathione-Sepharose beads (GE Healthcare) and mixed at 4 °C for 2 h. The beads were washed five times with binding buffer, resuspended in 30 μl of 2× SDS-PAGE loading buffer, and subjected to Western blot analysis.

Expression and purification of recombinant proteins

Single colonies of transformed Transetta(DE3) (TransGen Biotech) cells were maintained at 37 °C in LB medium containing kanamycin (50 μg/ml) with constant shaking. When the A_{600} of cultures reached 0.6–0.8, the cultures were chilled for 30 min on ice, IPTG was added to a final concentration of 0.2 mM, and the cultures were incubated for 18 h at 18 °C with constant shaking. Cells were harvested by centrifugation at 4000 rpm for 10 min and stored at −80 °C. Protein purification was performed as described previously with some modifications (83). The following operations were performed at 4 °C. Cell pellets were suspended by vortexing in 5 ml of lysis buffer (50 mM HEPES-NaOH, pH 7.5, 600 mM NaCl, 2 mM β-mercaptoethanol, 20 mM imidazole, and 10% (v/v) glycerol)/1 g of cells with PMSF (Sigma) and lysed by ultrasonication. Insoluble material was removed by centrifugation for 40 min at 13,200 × *g*. The supernatant was applied to HisTrap HP columns (GE Healthcare) pre-equilibrated with lysis buffer using the Äkta Prime system (GE Healthcare). Unspecifically bound proteins were removed by washing with 10 column volumes (CV) of lysis buffer followed by 2 CV of washing buffer (20 mM HEPES-NaOH, pH 7.5, 2 M LiCl, 5% glycerol) to remove nucleic acid and further by 2 CV of lysis buffer. Bound proteins were eluted with a 20-CV gradient of 20–100% elution buffer (50 mM HEPES-NaOH, pH 7.5, 600 mM NaCl, 2 mM β-mercaptoethanol, 250 mM imidazole, 10% (v/v) glycerol). Elution of the proteins was monitored by SDS-PAGE analysis of the obtained fractions. The elution buffers were exchanged by dialysis against lysis buffer containing 20 mM imidazol. The His-SUMO tags were cleaved with Ulp1. Proteins were then applied again onto affinity columns to remove cleaved tags and proteases, and purified proteins without tags were collected in the flow-through. Proteins were concentrated using an Amicon Ultra-15 centrifugal filter unit (Millipore) and further purified by size exclusion chromatography (GE Healthcare) using buffers containing 20 mM HEPES-NaOH, pH 7.5, 200 mM NaCl, 2 mM DTT, and 5% (v/v) glycerol.

ATPase assay

The ATPase activity of the proteins (100 nM hPrp43 with or without 500 nM of RNA_{40} and 100 nM ZIP or ZIPΔG-patch) was measured at 0.01, 0.1, and 0.5 mM ATP (Thermo Scientific Pierce) in 30 °C with a QuantiChrom™ ATPase/GTPase assay

kit (BioAssay Systems) according to the manufacturer's instruction. The RNA_{40} sequence was 5′-GCCGCCGUUCUCCUGGAUCCAUAGGCACUGAGUUGGUAUG-3′ as described previously (84).

Helicase assay

3′- and 5′-tailed RNA/DNA substrates were prepared as described previously with some modifications (39). Briefly, a 98-nucleotide RNA strand, 5′-GGGAGACCCAAGCUGGCUAGCGUUUAAACGGGCCCUCUAGACUCGAGCGGCCGCCACUGUGCUGGAUAUCUGCAGAAUUCCACCACACUGGACUAGUG-3′, was synthesized by *in vitro* transcription from a BamH I linearized pcDNA3.1(−) vector and annealed to biotin-labeled DNA oligonucleotides, 5′-CGCTAGCCAGCTTGGGTCTCCC-biotin-3′ to generate a 3′-tailed 22-bp duplex and 5′-biotin-CACTAGTCCAGTGTGGTGGAATTCTGC-3′ to yield a 5′-tailed 27-bp duplex. The relative stability of the 22-bp RNA/DNA duplex with a 3′ overhang, calculated using nearest-neighbor parameters (85), was −37.2 kcal/mol, similar to that of the 5′-tailed 27-bp duplex (−37.4 kcal/mol). The annealed substrates were gel-purified by 6% native PAGE. The reaction mixtures (10 μl) (3′- or 5′-tailed RNA/DNA substrate, 100 nM hPrp43 and 100 nM ZIP or ZIPΔG-patch, 40 mM Tris-HCl, pH 7.0, 2 mM DTT, 250 nM excessive unlabeled antisense DNA oligonucleotide) were preincubated for 15 min on ice followed by the addition of 1 mM ATP and incubation at 30 °C. The reactions were stopped 40 min later by the addition of 2 μl of a solution containing 1 mg/ml proteinase K, 1.25% SDS, 50 mM Tris-HCl, pH 7.4, 0.06% bromphenol blue, 0.06% xylene cyanol, and 30% glycerol. The samples were resolved by electrophoresis on an 8% native polyacrylamide gel using 1× TBE as running buffer, transferred onto nylon membrane, and then detected using a chemiluminescent nucleic acid detection module kit.

Statistical analysis

The bands were quantified by densitometry with ImageJ software. The results were reported as mean ± S.D., and the statistical analysis was performed using an unpaired two-tailed *t* test between control and experimental groups with $p < 0.05$ considered statistically significant.

Author contributions—Z. C. and Y. S. designed the experiments, interpreted the data, and wrote the paper. Z. C., B. G., Y. Z., G. X., W. L., S. L., B. X., C. W., L. H., J. Y., X. Y., X. Y., L. S., and J. L. carried out the experiments.

References

1. Wahl, M. C., Will, C. L., and Lührmann, R. (2009) The spliceosome: Design principles of a dynamic RNP machine. *Cell* **136,** 701–718
2. Will, C. L., and Lührmann, R. (2011) Spliceosome structure and function. *Cold Spring Harb. Perspect. Biol.* **3,** a003707
3. Will, C. L., and Lührmann, R. (2001) Spliceosomal UsnRNP biogenesis, structure and function. *Curr. Opin. Cell Biol.* **13,** 290–301
4. Patel, S. B., and Bellini, M. (2008) The assembly of a spliceosomal small nuclear ribonucleoprotein particle. *Nucleic Acids Res.* **36,** 6482–6493
5. Matera, A. G., and Wang, Z. (2014) A day in the life of the spliceosome. *Nat. Rev. Mol. Cell Biol.* **15,** 108–121
6. Krämer, A., Keller, W., Appel, B., and Lührmann, R. (1984) The 5′ terminus of the RNA moiety of U1 small nuclear ribonucleoprotein particles is required for the splicing of messenger RNA precursors. *Cell* **38,** 299–307
7. Black, D. L., Chabot, B., and Steitz, J. A. (1985) U2 as well as U1 small nuclear ribonucleoproteins are involved in premessenger RNA splicing. *Cell* **42,** 737–750
8. Zhuang, Y., and Weiner, A. M. (1986) A compensatory base change in U1 snRNA suppresses a 5′ splice site mutation. *Cell* **46,** 827–835
9. Parker, R., Siliciano, P. G., and Guthrie, C. (1987) Recognition of the TACTAAC box during mRNA splicing in yeast involves base pairing to the U2-like snRNA. *Cell* **49,** 229–239
10. Zhuang, Y., and Weiner, A. M. (1989) A compensatory base change in human U2 snRNA can suppress a branch site mutation. *Genes Dev.* **3,** 1545–1552
11. Bindereif, A., and Green, M. R. (1987) An ordered pathway of snRNP binding during mammalian pre-mRNA splicing complex assembly. *EMBO J.* **6,** 2415–2424
12. Cheng, S. C., and Abelson, J. (1987) Spliceosome assembly in yeast. *Genes Dev.* **1,** 1014–1027
13. Konarska, M. M., and Sharp, P. A. (1987) Interactions between small nuclear ribonucleoprotein particles in formation of spliceosomes. *Cell* **49,** 763–774
14. Madhani, H. D., and Guthrie, C. (1992) A novel base-pairing interaction between U2 and U6 snRNAs suggests a mechanism for the catalytic activation of the spliceosome. *Cell* **71,** 803–817
15. Sawa, H., and Shimura, Y. (1992) Association of U6 snRNA with the 5′-splice site region of pre-mRNA in the spliceosome. *Genes Dev.* **6,** 244–254
16. Wassarman, D. A., and Steitz, J. A. (1992) Interactions of small nuclear RNA's with precursor messenger RNA during *in vitro* splicing. *Science* **257,** 1918–1925
17. Tarn, W. Y., Lee, K. R., and Cheng, S. C. (1993) Yeast precursor mRNA processing protein PRP19 associates with the spliceosome concomitant with or just after dissociation of U4 small nuclear RNA. *Proc. Natl. Acad. Sci. U.S.A.* **90,** 10821–10825
18. Tarn, W. Y., Hsu, C. H., Huang, K. T., Chen, H. R., Kao, H. Y., Lee, K. R., and Cheng, S. C. (1994) Functional association of essential splicing factor(s) with PRP19 in a protein complex. *EMBO J.* **13,** 2421–2431
19. Chan, S. P., Kao, D. I., Tsai, W. Y., and Cheng, S. C. (2003) The Prp19p-associated complex in spliceosome activation. *Science* **302,** 279–282
20. Staley, J. P., and Guthrie, C. (1998) Mechanical devices of the spliceosome: Motors, clocks, springs, and things. *Cell* **92,** 315–326
21. Fourmann, J. B., Schmitzová, J., Christian, H., Urlaub, H., Ficner, R., Boon, K. L., Fabrizio, P., and Lührmann, R. (2013) Dissection of the factor requirements for spliceosome disassembly and the elucidation of its dissociation products using a purified splicing system. *Genes Dev.* **27,** 413–428
22. Theuser, M., Höbartner, C., Wahl, M. C., and Santos, K. F. (2016) Substrate-assisted mechanism of RNP disruption by the spliceosomal Brr2 RNA helicase. *Proc. Natl. Acad. Sci. U.S.A.* **113,** 7798–7803
23. Raghunathan, P. L., and Guthrie, C. (1998) A spliceosomal recycling factor that reanneals U4 and U6 small nuclear ribonucleoprotein particles. *Science* **279,** 857–860
24. Bell, M., Schreiner, S., Damianov, A., Reddy, R., and Bindereif, A. (2002) p110, a novel human U6 snRNP protein and U4/U6 snRNP recycling factor. *EMBO J.* **21,** 2724–2735
25. Didychuk, A. L., Montemayor, E. J., Brow, D. A., and Butcher, S. E. (2016) Structural requirements for protein-catalyzed annealing of U4 and U6 RNAs during di-snRNP assembly. *Nucleic Acids Res.* **44,** 1398–1410
26. Stank, D., Rader, S. D., Klingauf, M., and Neugebauer, K. M. (2003) Targeting of U4/U6 small nuclear RNP assembly factor SART3/p110 to Cajal bodies. *J. Cell Biol.* **160,** 505–516
27. Stank, D., and Neugebauer, K. M. (2004) Detection of snRNP assembly intermediates in Cajal bodies by fluorescence resonance energy transfer. *J. Cell Biol.* **166,** 1015–1025
28. Schaffert, N., Hossbach, M., Heintzmann, R., Achsel, T., and Lührmann, R. (2004) RNAi knockdown of hPrp31 leads to an accumulation of U4/U6 di-snRNPs in Cajal bodies. *EMBO J.* **23,** 3000–3009
29. Novotny, I., Malinova, A., Stejskalova, E., Mateju, D., Klimesova, K., Roithova, A., Sveda, M., Knejzlik, Z., and Stanek, D. (2015) SART3-depen-

dent accumulation of incomplete spliceosomal snRNPs in Cajal bodies. *Cell Rep*. **10,** 429–440
30. Achsel, T., Brahms, H., Kastner, B., Bachi, A., Wilm, M., and Lührmann, R. (1999) A doughnut-shaped heteromer of human Sm-like proteins binds to the 3′-end of U6 snRNA, thereby facilitating U4/U6 duplex formation *in vitro*. *EMBO J.* **18,** 5789–5802
31. Nottrott, S., Urlaub, H., and Lührmann, R. (2002) Hierarchical, clustered protein interactions with U4/U6 snRNA: A biochemical role for U4/U6 proteins. *EMBO J.* **21,** 5527–5538
32. Behrens, S. E., and Lührmann, R. (1991) Immunoaffinity purification of a [U4/U6.U5] tri-snRNP from human cells. *Genes Dev.* **5,** 1439–1452
33. Liu, S., Rauhut, R., Vornlocher, H. P., and Luhrmann, R. (2006) The network of protein-protein interactions within the human U4/U6.U5 tri-snRNP. *RNA* **12,** 1418–1430
34. Li, R., Zhang, H., Yu, W., Chen, Y., Gui, B., Liang, J., Wang, Y., Sun, L., Yang, X., Zhang, Y., Shi, L., Li, Y., and Shang, Y. (2009) ZIP: A novel transcription repressor, represses *EGFR* oncogene and suppresses breast carcinogenesis. *EMBO J.* **28,** 2763–2776
35. Brown, R. S. (2005) Zinc finger proteins: Getting a grip on RNA. *Curr. Opin. Struct. Biol.* **15,** 94–98
36. Hall, T. M. (2005) Multiple modes of RNA recognition by zinc finger proteins. *Curr. Opin. Struct. Biol.* **15,** 367–373
37. Silverman, E. J., Maeda, A., Wei, J., Smith, P., Beggs, J. D., and Lin, R. J. (2004) Interaction between a G-patch protein and a spliceosomal DEXD/H-box ATPase that is critical for splicing. *Mol. Cell Biol.* **24,** 10101–10110
38. Tsai, R. T., Fu, R. H., Yeh, F. L., Tseng, C. K., Lin, Y. C., Huang, Y. H., and Cheng, S. C. (2005) Spliceosome disassembly catalyzed by Prp43 and its associated components Ntr1 and Ntr2. *Genes Dev.* **19,** 2991–3003
39. Tanaka, N., Aronova, A., and Schwer, B. (2007) Ntr1 activates the Prp43 helicase to trigger release of lariat-intron from the spliceosome. *Genes Dev.* **21,** 2312–2325
40. Warkocki, Z., Schneider, C., Mozaffari-Jovin, S., Schmitzová, J., Höbartner, C., Fabrizio, P., and Lührmann, R. (2015) The G-patch protein Spp2 couples the spliceosome-stimulated ATPase activity of the DEAH-box protein Prp2 to catalytic activation of the spliceosome. *Genes Dev.* **29,** 94–107
41. Christian, H., Hofele, R. V., Urlaub, H., and Ficner, R. (2014) Insights into the activation of the helicase Prp43 by biochemical studies and structural mass spectrometry. *Nucleic Acids Res.* **42,** 1162–1179
42. Lebaron, S., Papin, C., Capeyrou, R., Chen, Y. L., Froment, C., Monsarrat, B., Caizergues-Ferrer, M., Grigoriev, M., and Henry, Y. (2009) The ATPase and helicase activities of Prp43p are stimulated by the G-patch protein Pfa1p during yeast ribosome biogenesis. *EMBO J.* **28,** 3808–3819
43. Robert-Paganin, J., Réty, S., and Leulliot, N. (2015) Regulation of DEAH/RHA helicases by G-patch proteins. *BioMed Res. Int.* **2015,** 931857
44. Singh, G., and Cooper, T. A. (2006) Minigene reporter for identification and analysis of cis elements and trans factors affecting pre-mRNA splicing. *BioTechniques* **41,** 177–181
45. Matlin, A. J., Clark, F., and Smith, C. W. (2005) Understanding alternative splicing: Towards a cellular code. *Nat. Rev. Mol. Cell Biol.* **6,** 386–398
46. Chen, M., and Manley, J. L. (2009) Mechanisms of alternative splicing regulation: Insights from molecular and genomics approaches. *Nat. Rev. Mol. Cell Biol.* **10,** 741–754
47. Fu, X. D., and Ares, M., Jr. (2014) Context-dependent control of alternative splicing by RNA-binding proteins. *Nat. Rev. Genet.* **15,** 689–701
48. Arenas, J. E., and Abelson, J. N. (1997) Prp43: An RNA helicase-like factor involved in spliceosome disassembly. *Proc. Natl. Acad. Sci. U.S.A.* **94,** 11798–11802
49. Martin, A., Schneider, S., and Schwer, B. (2002) Prp43 is an essential RNA-dependent ATPase required for release of lariat-intron from the spliceosome. *J. Biol. Chem.* **277,** 17743–17750
50. Lebaron, S., Froment, C., Fromont-Racine, M., Rain, J. C., Monsarrat, B., Caizergues-Ferrer, M., and Henry, Y. (2005) The splicing ATPase prp43p is a component of multiple preribosomal particles. *Mol. Cell Biol.* **25,** 9269–9282
51. Combs, D. J., Nagel, R. J., Ares, M., Jr, and Stevens, S. W. (2006) Prp43p is a DEAH-box spliceosome disassembly factor essential for ribosome biogenesis. *Mol. Cell Biol.* **26,** 523–534
52. Leeds, N. B., Small, E. C., Hiley, S. L., Hughes, T. R., and Staley, J. P. (2006) The splicing factor Prp43p, a DEAH box ATPase, functions in ribosome biogenesis. *Mol. Cell Biol.* **26,** 513–522
53. Will, C. L., Urlaub, H., Achsel, T., Gentzel, M., Wilm, M., and Lührmann, R. (2002) Characterization of novel SF3b and 17S U2 snRNP proteins, including a human Prp5p homologue and an SF3b DEAD-box protein. *EMBO J.* **21,** 4978–4988
54. Makarov, E. M., Makarova, O. V., Achsel, T., and Lührmann, R. (2000) The human homologue of the yeast splicing factor prp6p contains multiple TPR elements and is stably associated with the U5 snRNP via protein-protein interactions. *J. Mol. Biol.* **298,** 567–575
55. Makarova, O. V., Makarov, E. M., and Lührmann, R. (2001) The 65 and 110 kDa SR-related proteins of the U4/U6.U5 tri-snRNP are essential for the assembly of mature spliceosomes. *EMBO J.* **20,** 2553–2563
56. Fabrizio, P., Laggerbauer, B., Lauber, J., Lane, W. S., and Lührmann, R. (1997) An evolutionarily conserved U5 snRNP-specific protein is a GTP-binding factor closely related to the ribosomal translocase EF-2. *EMBO J.* **16,** 4092–4106
57. Kastner, B., Fischer, N., Golas, M. M., Sander, B., Dube, P., Boehringer, D., Hartmuth, K., Deckert, J., Hauer, F., Wolf, E., Uchtenhagen, H., Urlaub, H., Herzog, F., Peters, J. M., Poerschke, D., Lührmann, R., and Stark, H. (2008) GraFix: Sample preparation for single-particle electron cryomicroscopy. *Nat. Methods* **5,** 53–55
58. Stanek, D., Pridalová-Hnilicová, J., Novotný, I., Huranová, M., Blazíková, M., Wen, X., Sapra, A. K., and Neugebauer, K. M. (2008) Spliceosomal small nuclear ribonucleoprotein particles repeatedly cycle through Cajal bodies. *Mol. Biol. Cell* **19,** 2534–2543
59. Andrade, L. E., Chan, E. K., Raska, I., Peebles, C. L., Roos, G., and Tan, E. M. (1991) Human autoantibody to a novel protein of the nuclear coiled body: Immunological characterization and cDNA cloning of p80-coilin. *J. Exp. Med.* **173,** 1407–1419
60. Fouraux, M. A., Kolkman, M. J., Van der Heijden, A., De Jong, A. S., Van Venrooij, W. J., and Pruijn, G. J. (2002) The human La (SS-B) autoantigen interacts with DDX15/hPrp43, a putative DEAH-box RNA helicase. *RNA* **8,** 1428–1443
61. Klingauf, M., Stanek, D., and Neugebauer, K. M. (2006) Enhancement of U4/U6 small nuclear ribonucleoprotein particle association in Cajal bodies predicted by mathematical modeling. *Mol. Biol. Cell* **17,** 4972–4981
62. Novotný, I., Blažíková, M., Staněk, D., Herman, P., and Malinsky, J. (2011) *In vivo* kinetics of U4/U6.U5 tri-snRNP formation in Cajal bodies. *Mol. Biol. Cell* **22,** 513–523
63. Liu, S., Mozaffari-Jovin, S., Wollenhaupt, J., Santos, K. F., Theuser, M., Dunin-Horkawicz, S., Fabrizio, P., Bujnicki, J. M., Lührmann, R., and Wahl, M. C. (2015) A composite double-/single-stranded RNA-binding region in protein Prp3 supports tri-snRNP stability and splicing. *eLife* **4,** e07320
64. Nguyen, T. H. D., Galej, W. P., Bai, X. C., Oubridge, C., Newman, A. J., Scheres, S. H. W., and Nagai, K. (2016) Cryo-EM structure of the yeast U4/U6.U5 tri-snRNP at 3.7 A resolution. *Nature* **530,** 298–302
65. Wan, R., Yan, C., Bai, R., Wang, L., Huang, M., Wong, C. C., and Shi, Y. (2016) The 3.8 A structure of the U4/U6.U5 tri-snRNP: Insights into spliceosome assembly and catalysis. *Science* **351,** 466–475
66. Agafonov, D. E., Kastner, B., Dybkov, O., Hofele, R. V., Liu, W. T., Urlaub, H., Lührmann, R., and Stark, H. (2016) Molecular architecture of the human U4/U6.U5 tri-snRNP. *Science* **351,** 1416–1420
67. Medenbach, J., Schreiner, S., Liu, S., Lührmann, R., and Bindereif, A. (2004) Human U4/U6 snRNP recycling factor p110: mutational analysis reveals the function of the tetratricopeptide repeat domain in recycling. *Mol. Cell Biol.* **24,** 7392–7401
68. Niu, Z., Jin, W., Zhang, L., and Li, X. (2012) Tumor suppressor RBM5 directly interacts with the DExD/H-box protein DHX15 and stimulates its helicase activity. *FEBS Lett.* **586,** 977–983
69. Warzecha, C. C., Sato, T. K., Nabet, B., Hogenesch, J. B., and Carstens, R. P. (2009) ESRP1 and ESRP2 are epithelial cell-type-specific regulators of FGFR2 splicing. *Mol. Cell* **33,** 591–601
70. Bach, M., Winkelmann, G., and Lührmann, R. (1989) 20S small nuclear ribonucleoprotein U5 shows a surprisingly complex protein composition. *Proc. Natl. Acad. Sci. U.S.A.* **86,** 6038–6042

71. Koodathingal, P., Novak, T., Piccirilli, J. A., and Staley, J. P. (2010) The DEAH box ATPases Prp16 and Prp43 cooperate to proofread 5′ splice site cleavage during pre-mRNA splicing. *Mol. Cell* **39,** 385–395
72. Mayas, R. M., Maita, H., Semlow, D. R., and Staley, J. P. (2010) Spliceosome discards intermediates via the DEAH box ATPase Prp43p. *Proc. Natl. Acad. Sci. U.S.A.* **107,** 10020–10025
73. Lin, M. L., Fukukawa, C., Park, J. H., Naito, K., Kijima, K., Shimo, A., Ajiro, M., Nishidate, T., Nakamura, Y., and Katagiri, T. (2009) Involvement of G-patch domain containing 2 overexpression in breast carcinogenesis. *Cancer Sci.* **100,** 1443–1450
74. Bohnsack, M. T., Martin, R., Granneman, S., Ruprecht, M., Schleiff, E., and Tollervey, D. (2009) Prp43 bound at different sites on the pre-rRNA performs distinct functions in ribosome synthesis. *Mol. Cell* **36,** 583–592
75. Young, P. J., Le, T. T., thi Man, N., Burghes, A. H., and Morris, G. E. (2000) The relationship between SMN, the spinal muscular atrophy protein, and nuclear coiled bodies in differentiated tissues and cultured cells. *Exp. Cell Res.* **256,** 365–374
76. Collier, S., Pendle, A., Boudonck, K., van Rij, T., Dolan, L., and Shaw, P. (2006) A distant coilin homologue is required for the formation of Cajal bodies in *Arabidopsis*. *Mol. Biol. Cell* **17,** 2942–2951
77. Liu, J. L., Wu, Z., Nizami, Z., Deryusheva, S., Rajendra, T. K., Beumer, K. J., Gao, H., Matera, A. G., Carroll, D., and Gall, J. G. (2009) Coilin is essential for Cajal body organization in *Drosophila melanogaster*. *Mol. Biol. Cell* **20,** 1661–1670
78. Tucker, K. E., Berciano, M. T., Jacobs, E. Y., LePage, D. F., Shpargel, K. B., Rossire, J. J., Chan, E. K., Lafarga, M., Conlon, R. A., and Matera, A. G. (2001) Residual Cajal bodies in coilin knockout mice fail to recruit Sm snRNPs and SMN, the spinal muscular atrophy gene product. *J. Cell Biol.* **154,** 293–307
79. Walker, M. P., Tian, L., and Matera, A. G. (2009) Reduced viability, fertility and fecundity in mice lacking the Cajal body marker protein, coilin. *PLoS ONE* **4,** e6171
80. Cartegni, L., Wang, J., Zhu, Z., Zhang, M. Q., and Krainer, A. R. (2003) ESEfinder: A Web resource to identify exonic splicing enhancers. *Nucleic Acids Res.* **31,** 3568–3571
81. van Heel, M., Harauz, G., Orlova, E. V., Schmidt, R., and Schatz, M. (1996) A new generation of the IMAGIC image processing system. *J. Struct. Biol.* **116,** 17–24
82. Sander, B., Golas, M. M., Makarov, E. M., Brahms, H., Kastner, B., Lührmann, R., and Stark, H. (2006) Organization of core spliceosomal components U5 snRNA loop I and U4/U6 Di-snRNP within U4/U6.U5 Tri-snRNP as revealed by electron cryomicroscopy. *Mol. Cell* **24,** 267–278
83. Warkocki, Z., Odenwälder, P., Schmitzová, J., Platzmann, F., Stark, H., Urlaub, H., Ficner, R., Fabrizio, P., and Lührmann, R. (2009) Reconstitution of both steps of *Saccharomyces cerevisiae* splicing with purified spliceosomal components. *Nat. Struct. Mol. Biol.* **16,** 1237–1243
84. Tanaka, N., and Schwer, B. (2006) Mutations in PRP43 that uncouple RNA-dependent NTPase activity and pre-mRNA splicing function. *Biochemistry* **45,** 6510–6521
85. Sugimoto, N., Nakano, S., Katoh, M., Matsumura, A., Nakamuta, H., Ohmichi, T., Yoneyama, M., and Sasaki, M. (1995) Thermodynamic parameters to predict stability of RNA/DNA hybrid duplexes. *Biochemistry* **34,** 11211–11216